An Integrated Geospatial Approach of GHG Emission Impact on Air Quality Due to Above-Ground Biomass in Rawalpindi Division, Punjab, Pakistan

Hira Shahbaz, Shakeel Mahmood, Kanwal Javid
Department of Geography, Government College University, Lahore, Pakistan
Correspondence: hira72370@gmail.com , shakeelmahmood@gcu.edu.pk

Citation | Shahbaz. H, Mahmood. S, Javid. K, "An Integrated Geospatial Approach of GHG Emission Impact on Air Quality Due to Above-Ground Biomass in Rawalpindi Division, Punjab, Pakistan", IJIST, Special Issue pp 330-355, August 2025.
Received| August 03, 2025 **Revised**| August 21, 2025 **Accepted**| August 22, 2025 **Published**| August 23, 2025.

This study investigates the influence of above-ground biomass (AGB) on greenhouse gas (GHG) emissions and air quality in the Rawalpindi Division, Punjab, Pakistan, from 2018 to 2024. An integrated geospatial approach was applied using Sentinel-2 for vegetation indices, Sentinel-3 for land surface temperature (LST), Sentinel-5P for atmospheric pollutants, and MODIS for active fire detection. Results indicate that while high AGB zones expanded, moderate and low biomass areas declined, suggesting biomass redistribution due to vegetation change. Fire radiative power (FRP) was strongly correlated with AGB (R^2 = 0.9888), indicating that biomass burning significantly contributed to pollutant concentrations. Linear regression showed strong positive correlations between AGB and NDVI (R^2 = 0.89), LST (R^2 = 0.96), and GHGs, including CO_2, CO, NO_2, SO_2, aerosols, and ozone. Notably, LST and pollutant levels peaked during dry seasons. The findings emphasize the dual role of biomass as a carbon sink and emission source, highlighting the utility of remote sensing for environmental monitoring and climate planning.

Keywords: AGB, Remote Sensing, Fire Radiative Power, NDVI, GHG Emissions

Introduction:

Bioenergy is a sustainable energy source that comes from organic matter, often known as biomass, that comes from living or recently living (as opposed to fossil) organisms[1]Carbon emissions from deforestation and forest degradation can impact the global climate and cause environmental change [2] Forest biomass research is crucial for monitoring the carbon cycles of terrestrial ecosystems, which provide essential data for understanding climate change [3] It is possible to quantify the reserves and carbon capture rates of forest ecosystems through biomass estimation and monitoring.[4] The United Nations Program's Intergovernmental Panel on Climate Change (IPCC) states that the following locations comprise the majority of carbon stocks in forest ecosystems: woody debris, soil organic matter, forest litter layer, below-ground biomass, and above-ground biomass (AGB)[5]

Trees facilitate carbon storage, oxygen production, soil protection, and water cycle regulation. They sustain both human and natural food systems, offer homes to a wide variety of creatures, including humans, and supply building materials. Because of their vital role in the terrestrial environment, forests—including trees—are the best air purifiers. Without forests, it would be difficult for humans and other species to survive on Earth [6], Burning fossil fuels, deforestation, and industrial operations are the main human activities that emit greenhouse gases such as carbon dioxide (CO_2), methane (CH_4), and nitrous oxide (N_2O). In Southeast Asia, biomass burning from forest fires and the burning of agricultural waste has been a significant problem that has an impact on aquatic ecosystems, land use, human health, and air visibility. The upper layers of the atmosphere were warmed by light-absorbing smoke particles, which decreased surface evaporation and stopped convection, which was a crucial component of the hydrological cycle. Burning biomass was responsible for over 50% of elemental carbon and two-thirds of all organic carbon in South Asia [7]. Since these gases are detrimental to the ecosystem, human health, and the environment worldwide, quick action is required to lessen their effects[8] Human health is one of the most important concerns as a result of environmental degradation**,** including problems like ecological and climate change, greenhouse gas emissions, deforestation, biodiversity loss, disturbance of the water cycle, soil erosion, desertification, changes in temperature and precipitation, and fluctuations in economic growth [9] Emissions of carbon dioxide and other greenhouse gases have increased to alarming levels worldwide. Understanding how carbon dioxide emissions from different sectors affect environmental sustainability in Pakistan is essential, given the country's increasing urbanization, industry, and energy consumption. [10] Pakistan makes up only 0.5% of CO_2 emissions and 0.9% of global greenhouse gas emissions. However, to meet its energy needs, the nation mainly depends on fossil fuels, including coal, gas, and petroleum products. Crude oil accounted for 19.9% of the energy supply in 2021, followed by gas (20.0%), coal (13.7%), and nuclear power (3.3%). About 38.5% of Pakistan's CO_2 emissions came from oil, 30.4% from natural gas, and 31.1% from coal [11] With plans to raise the proportion of renewable energy to 60% by 2030, Pakistan also has significant potential for renewable energy sources, including solar, wind, and hydropower through the China-Pakistan Economic Corridor (CPEC) initiative. China has invested heavily in renewable energy projects in Pakistan [12] This study assesses the biomass from vegetation indices and its impact on CO_2 emissions in the Punjab Division, Rawalpindi**,** including greenhouse gases such as NO_2, SO_2, CO, O_3, and aerosol-caused air pollution by biomass, liquid, and solid fuel consumption, residential buildings, commercial and public services, and transportation.

A vital part of the carbon cycle is above-ground biomass (AGB). In addition to being the third largest producer of CO_2 emissions, it is the primary sink of carbon that is above ground on Earth. As a natural regulator of climate change and a significant contributor to the global carbon budget, tropical forests are crucial in storing and sequestering vast amounts of

carbon [5] Vegetation biomass is an all-encompassing variable that is linked to numerous elements, such as the species composition, density, and stand structure of the vegetation. In semiarid regions, rainfall has a significant impact on the growth of vegetation biomass [13] On the other hand, because remote sensing techniques can provide information at a variety of spatial and temporal scales, wall-to-wall coverage, frequent "revisits" of the area, and use as historical data archives, they can provide spatially explicit and more effectively combined forest biomass estimates [14] Despite significant advances in estimating above-ground biomass (AGB) and greenhouse gas (GHG) emissions using remote sensing, most studies in Pakistan focus either on biomass estimation or air pollution monitoring in isolation. Limited work has integrated multi-sensor remote sensing data to explore the spatial-temporal interactions between biomass dynamics, fire activity, and pollutant concentrations. This research addresses this gap by applying a geospatial approach combining Sentinel-2, Sentinel-3, Sentinel-5P, MODIS, and statistical methods to investigate how AGB changes relate to air pollutant levels in Rawalpindi Division from 2018–2024 [15] In light of Pakistan's increasing energy demand and the environmental burden of fossil fuel reliance, sustainable biomass monitoring has become critical. This study leverages multi-sensor satellite data to evaluate AGB trends and their environmental implications. Specifically, the research uses Sentinel-2 data for vegetation indices, Sentinel-3 for LST, Sentinel-5P for pollutant mapping, and MODIS for active fires. The integrated analysis supports efforts to quantify biomass as both a carbon source and sink in the Rawalpindi Division. For the reasons listed above, a variety of technologies have been developed to detect and monitor different elements of aerosol emission, GHG, and active fire detection. The physical relationship between burning biomass and air pollution was captured by the study's findings, which will aid in pertinent air pollution management and control [7].

Study Area:

The Punjab province in Pakistan's Rawalpindi Division served as the study's location (Figure 1). Geographically, it is located between latitudes 32.414528 and 34.024395 North and longitudes 71.688324 E and 73.753807 E. The Rawalpindi Division is bordered to the north by the Kala-Chitta Ranges and Margalla Hills, to the west by the Indus River, and to the east by the Jhelum River. On the south side is the Salt Range. Its general elevation is from 472–610 meters above mean sea level, and its entire land area is approximately 22,254 km². In terms of administration, the division comprises 22 tehsils and 4 districts.

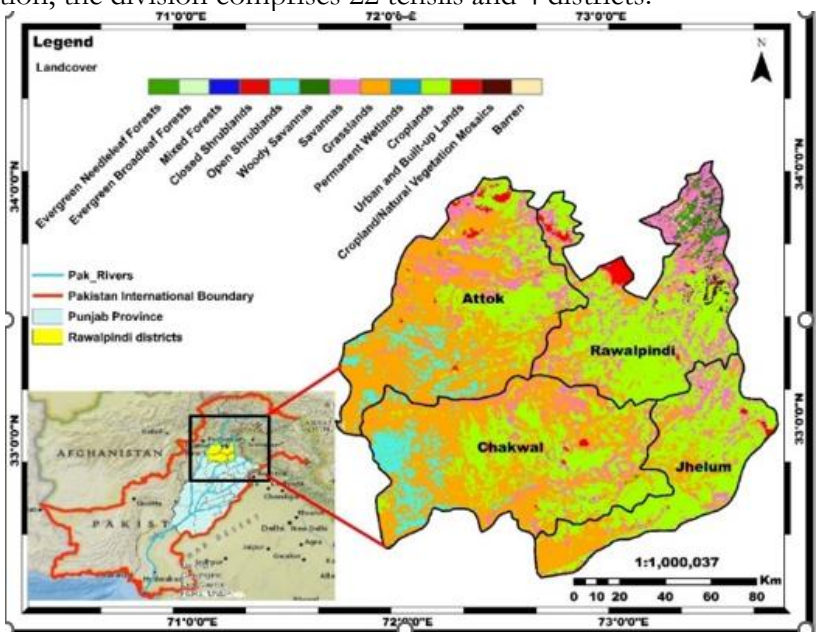

Figure 1. The study area

The climate of Rawalpindi Division is generally harsh, with regional variations ranging from hot to warm summers and pleasant to chilly winters. The annual rainfall varies greatly, ranging from 21 to more than 60 inches (Iqbal and Iqbal 2018). As of the 2017 census, the Rawalpindi Division has an approximate population of 10.01 million with moderate growth projected to 2024 [16](Pakistan Bureau of Statistics, 2017).

Objectives:

To analyze the spatial-temporal variation of forest and grassland biomass from vegetation indices by using remote sensing technology

To moniter the spatio-temporal variation of air pollutant concentration due to biomass burning.

To estimate the intensity of fire activity and burning areas and their relationship with biomass by using geospatial techniques.

To correlate the biomass and its influencing factors by using the pearson linear method

Material and Methods:

Data collection:

Sentinel-2 L2A, Sentinel-3 L2A Sentinel-5P products were downloaded from the Copernicus Open Access Hub (*https://scihub.copernicus.eu*, last accessed 16/10/2023). The publicly available high-resolution Sentinel-2 (S2) Level-2A product used in this study was obtained on October 16, 2022, which also happens to be the survey month. The Copernicus Open Access Hub website (*https://scihub.copernicus.eu/dhus*) provided the S2 dataset for download. With a 5-day revisit frequency and 12 spectral bands, Sentinel-2 enables vegetation monitoring at regional and global scales at several spatial resolutions (10, 20, and 60 m). Six red-edge and short-wave infrared bands have a spatial resolution of 20 m, two atmospheric bands have a spatial resolution of 60 m, and there are four visible and near-infrared (NIR) bands with a spatial resolution of 10 m.

The European Copernicus Program's first mission to provide measurements of atmospheric constituents with the goal of enhancing the European Union's ability to monitor air quality is the Tropospheric Monitoring Instrument TROPOMI Sentinel-5P, which was launched on October 13, 2017. Estimates of troposphere trace gases, such as NO_2, O_3, SO_2, and carbon monoxide (CO), along with aerosol and cloud indices, make up Level-2 products. Sentinel-3 satellites use the SLSTR to collect thermal data. With a spatial resolution of 1 km and revisit times of June and July for the years 2018 and 2024, SLSTR offers two TIR bands. The Soil Organic Carbon Stock has been obtained using the Soil website SoilGrids250m 2.0. MODIS NASA | LANCE | FIRMS is the source of the active fire data for June 26, 2024.

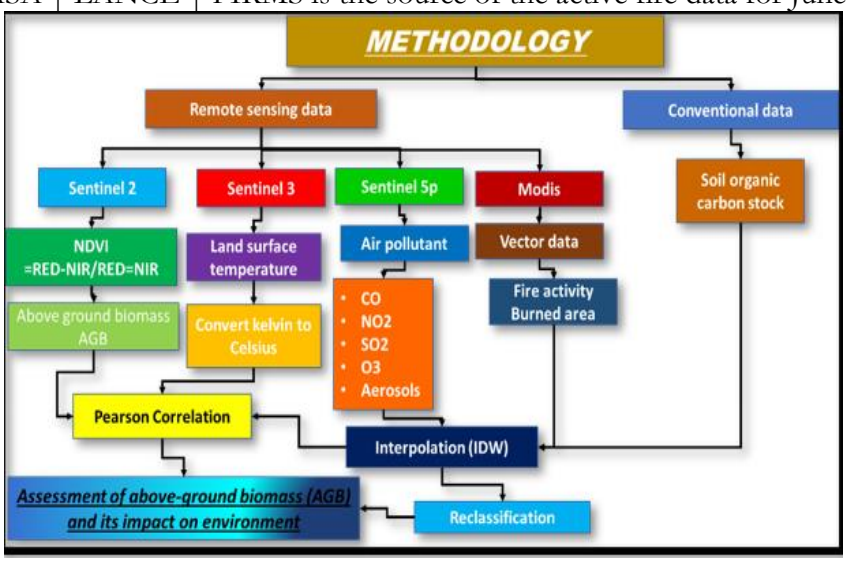

Figure 2. The methodological framework

Image Preprocessing:

The current project utilizes GIS to determine the study area's coordinate reference system (CRS) using EPSG:32646, which corresponds to WGS 84/UTM Zone 43N. Sensors and imaging equipment are used in remote sensing technologies for air pollution monitoring to identify and measure air contaminants. These technologies can be used to provide comprehensive coverage and data for air quality evaluation from satellites, airplanes, drones, and ground-based stations. They usually measure the coverage of pollutants like carbon monoxide (CO), nitrogen dioxide (NO2), sulfur dioxide (SO2), and ozone (O3), as well as the capacity to track long-term trends in large-scale air pollution.

Estimation of AGB Through Vegetation Indices:

By establishing the NDVI image threshold, the process was used to determine the study area's vegetation cover and the changes that took place over the reference period. Thus, only three visible bands—near infrared, visible green, and visible red—were used, and other features were retrieved with the help of the four visible arrays (middle infrared, visible blue, and thermal infrared). The Vegetation Index with Normalized Differences (NDVI) developed by [17] is a measure of photosynthetic activity and vegetation vigor. The Sentinel-2 sensor's red band (R) and near-infrared band (NIR) were used to estimate it. Using ArcGIS 10.8's mosaic tool, the obtained images from Sentinel-2 were mosaicked and then further processed to produce NDVI. The NDVI was computed using the following formula:

$$NDVI = RED\text{-}NIR/RED+NIR$$

The greatest biomass on Earth is known as above-ground biomass, or AGB. The greatest biomass on Earth is known as above-ground biomass (AGB)[18] As [2] stated, estimating biomass using remote sensing data is a difficult process that calls for meticulous planning of numerous processes. The tropical forest biomass and grassland biomass in this study were calculated from the NDVI using Sentinel 2 imagery and the following formulas:

Tropical forest biomass: AGB (Mg/ha) = 134.4*NDVI+21.1

Grassland biomass: AGB (kg/ha) = 43.8*NDVI+6.2

Land Surface Temperature (LST):

The study area's Sentinel-3 SLSTR data were retrieved, and the Kelvin-scale image LST values were converted to Celsius by subtracting 273.15. The procedure was carried out in the ArcGIS 10.7.1 raster calculator using the following equation:

$$C = K - 273.15$$

Air Pollutants:

Emissions from burning biomass clearly have an impact on air quality.[19] To order to comprehend how carbon emissions have changed over time, this study conducted a multi-temporal analysis[20]

Air pollutants Emissions from burning biomass have been shown to significantly affect air quality [19] To analyze changes in carbon emissions over time, a multi-temporal analysis was conducted[20]. Raster datasets were accessed through the Sentinel Hub EO Browser platform after user authentication. Sentinel-5P data layers including aerosol, carbon monoxide (CO), sulfur dioxide (SO_2), formaldehyde (HCHO), and nitrogen dioxide (NO_2) were downloaded in GeoTIFF format. Appropriate coordinate reference systems and spatial resolutions were assigned during preprocessing. The data were then interpolated using the IDW method to generate continuous spatial surfaces.

Active Fires Analysis:

The global Collection 5 MODIS 1 km Level 2 active fire product locates and times flames burning within 1 km of the NASA Terra (MOD14) and Aqua (MYD14) satellites passing overhead when there are no clouds. MODIS Active Fire data (Collection 5, 1 km resolution) were downloaded in JPEG format and georeferenced in ArcGIS using ground control points and EPSG:32646 projection. Vector shapefiles were created from the

georeferenced fire points, and fire radiative power (FRP) values were interpolated using the IDW technique. Burn area extent was estimated using change detection in vegetation indices, and emissions were quantified based on pixel-level analysis and statistical correlation with AGB.

Soil Organic Carbon (SOC):

The study area's soil organic carbon stock (SOC) in t/ha has been clipped using the extract-by-mask approach after the downloaded images of the SOC for each district of the Rawalpindi Division were combined using the mosaic to new raster tool.

Linear Regression analysis:

Finally, using biomass as the dependent variable and biomass-related parameters as the independent variable, linear regression analysis was utilized to assess the association between above-ground biomass and all parameters spatial temporal variation. The linear regression equation was applied for this purpose and is explained as follows:

$$Y = \alpha + \beta x$$

Were

Y = dependent variable value calculated by linear regression (biomass change)

α = the coefficient of freedom showing Y dependent on X.

β = the angle coefficient (slope) of the regression line, also reflecting the variation of Y variable when the X variable increases by one unit.

X = the independent variable

Additionally, R^2 is the variable Y's coefficient of determination in relation to the change of the variable X. The R^2 range is between 0 and 1. A higher R^2 value indicates that Y is dependent on X and changeable.

Results and Discussion:

Instead of restating visual content, the Results section now emphasizes the interpretation of spatial and temporal patterns. For example, in the NDVI analysis, high vegetation density in 2018 shifted to moderate and low categories by 2024, particularly in southern and central tehsils. This trend indicates urban expansion and vegetation stress likely driven by land-use change and climatic variation. In the LST analysis, rising surface temperatures were strongly associated with reduced vegetation, highlighting increased thermal stress and potential urban heat island effects in densely populated tehsils. Fire activity and FRP patterns reveal that biomass burning peaked in western zones, aligning with high-density fire points and explaining localized air quality deterioration. Air pollutant concentrations (e.g., NO_2, SO_2, CO) rose in tandem with AGB loss and FRP spikes, confirming the environmental cost of biomass combustion. These findings collectively support the correlation outcomes and validate the geospatial methodology.

Spatial-Temporal Distribution of Vegetation Cover (2018-2024):

In June, Rawalpindi's forest reaches its maximum level of vigor and greenness, resulting in exceptionally high NDVI values. Information about forest structure that is directly related to aboveground biomass may be shown differently in data gathered at different dates. Using NDVI, the current study looked at how urbanization has changed the forest and vegetation cover in the study area during the last six years.

(Figure 3) illustrates how the NDVI values in 2018 varied from 1 to -1. The northeastern portion of the division, which included the tehsils of Murree, Kotli Sattian, Kallar Syedan, and Kahuta, had the thickest forest cover, which was dominated by a rich green tint and covered 261.33 square kilometers. The southern part of the study region had a high level of forest cover, covering 566.52 square kilometers, whereas the northwest had a few isolated patches of moderate vegetation cover, covering 813.82 square kilometers. However, 222.66 and 66.33 sq km of area cover showed low and very low vegetation.

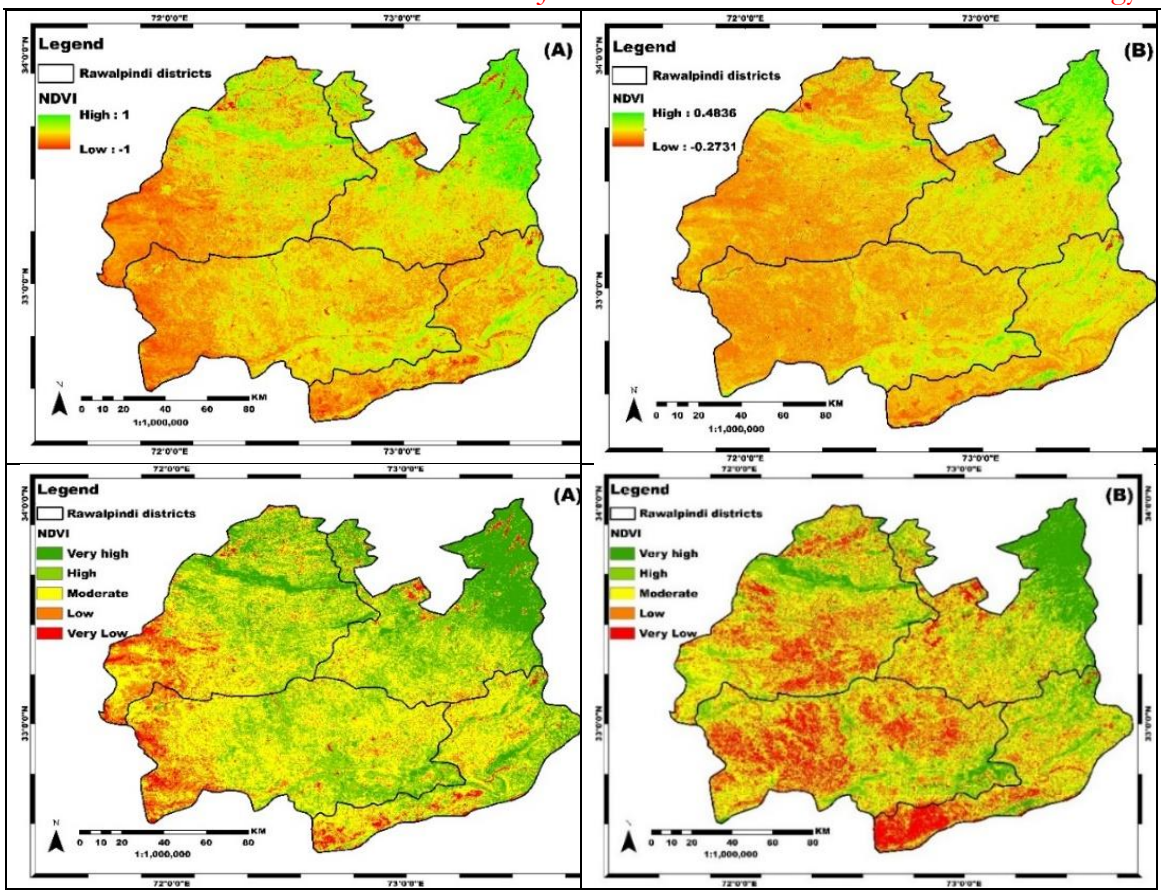

Figure 3. Spatial-temporal map of Normalized difference vegetation index (NDVI) (A) vegetation cover of 2018, (B) vegetation cover of 2024

The NDVI values for 2024 were also determined to be between 0.43 and -0.27. Murree, Kotli Sattian, Kahuta, and to a lesser extent Choa Saidan Shah were found to have relatively high and high vegetation cover**, with** areas of 184.79 and 408.89 sq km, respectively. Jand, Lawa, Pindi Gheb, Talagang**, ** and Fateh Jang, Sohawa, and Gujar Khan tehsils were the regions with the moderate, low, and very low NDVI values, which were 716.74, 376.87, and 243.62 sq km, respectively. According to Table 1**, ** the interpretation of the NDVI values**, ** shows that vegetation covers gradually decreased between 2018 and 2024

Table 1. Area calculation of NDVI (2018-2024)

Normalized Difference Vegetation Index (NDVI)			
2018		2024	
Area (Sqkm)	Area (%)	Area (Sqkm)	Area (%)
261.33	13.5358	184.79	9.5701
566.52	29.3433	408.89	21.176
813.82	42.1524	716.74	37.1193
222.66	11.5328	376.87	19.5177
66.33	3.43561	243.62	12.6168

Spatial-Temporal Distribution of Land Surface Temperature (2018-2024):

Many biotic and abiotic processes essential to plant growth depend on the temperature of the soil [21] Thermal infrared band data, which offer spectrum information on the energy exchange between solar radiation and the surface, can be used to determine the land surface temperature (LST)[17] The region in (Figure 5) experiences extremely low temperatures from 2018 to 2024, ranging from 46.33 sq km (2.39%) to 30.94 sq km (1.60%). Likewise, low land

surface temperature area cover dropped from 247 (12.79%) to 110.36 (5.71%) in 2018. In 2024, the area covered by the moderate surface temperature has increased to 529.94 (27.44%) from 458.1 (23.72%) in 2018. While the very high land surface temperature in 2018 covered an area of 444.54 and increased significantly in 2024 with an area coverage of 564.82 (29.25%), the high surface temperature in 2018 covered an area of 734.74 (38.05%) and decreased in 2024 with an area cover of 694.65 (35.975). According to the results (Table 2) of the spatial-temporal distribution, the land surface temperature increased progressively between 2018 and 2024.

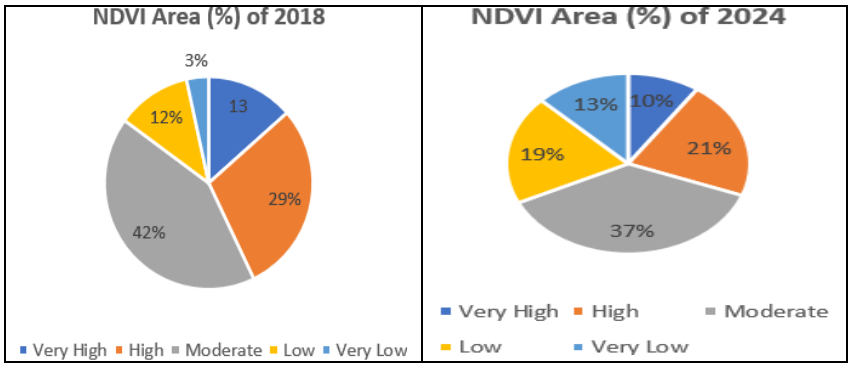

Figure 4. Graphical representation of NDVI area (2018-2024)

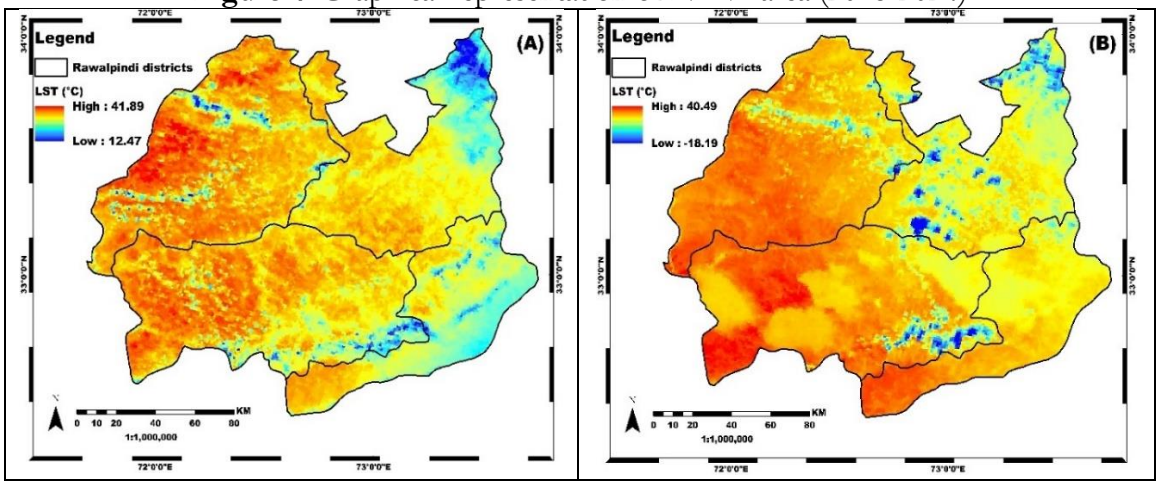

Figure 5. Spatial-temporal map of Land surface temperature (LST) (A) temperature of 2018 (B) temperature of 2024

Table 2. Area calculation of LST (2018-2024)

LST (°C)			
2018		2024	
Area (Sqkm)	Area (%)	Area (Sqkm)	Area (%)
46.33	2.39964	30.94	1.60252
247	12.7932	110.36	5.71603
458.1	23.727	529.94	27.4479
734.74	38.0554	694.65	35.979
444.54	23.0247	564.82	29.2545

Fire Activity Analysis:

Fire plays a role in ecosystem services; naturally produced wildfires are important for the sustainability of many terrestrial biomes and fire is one of nature's primary carbon-cycling mechanisms[22] Wildfires release globally significant amounts of aerosols, trace gases, and greenhouse gases that influence air quality, weather, and climate.

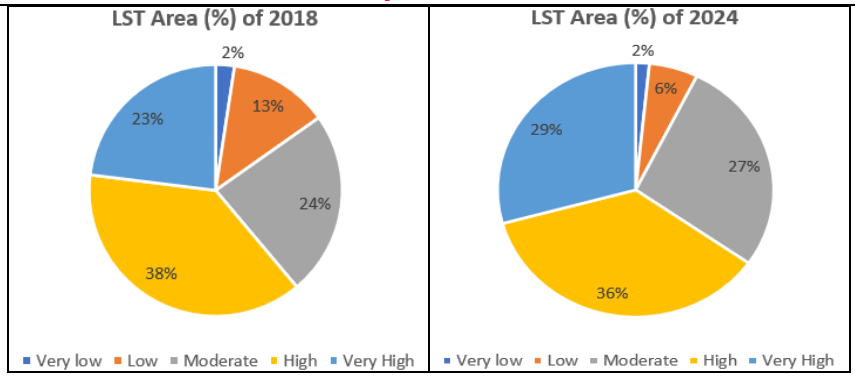

Figure 6. Graphical representation of LST area percentage (2018-2024**)**

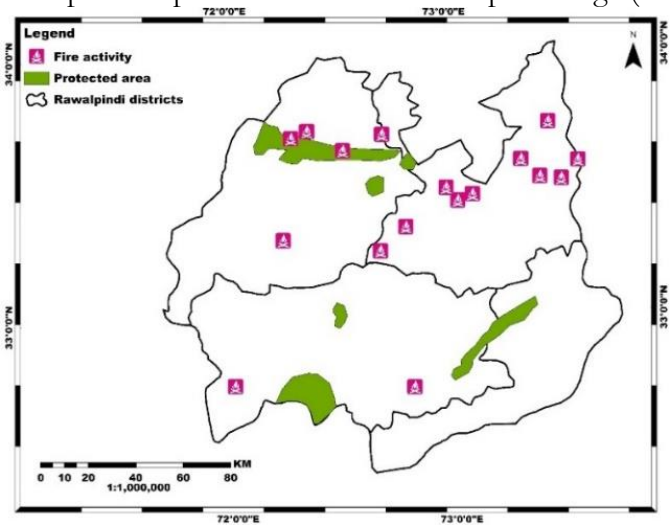

Figure 7. Fire activity map of Rawalpindi division

According to[23], the fire radiative energy (FRE), which has been demonstrated in (Figure 8) to be linearly related to the total amount of fuel burned by fire, is estimated by temporally integrating the FRP across the fire's life. By applying the point density at vector data of FRP the results illustrated from low (42.77 MW) to high (105.67 MW) density value range as The FRP is proportional to the rate of biomass consumption. Strong correlations were found (Figure 9) between the two products for the monthly total FRP aggregated from all detected fires in the fire products, with Rawalpindi's goodness of fit R-squared (R2) reaching 0.9888.

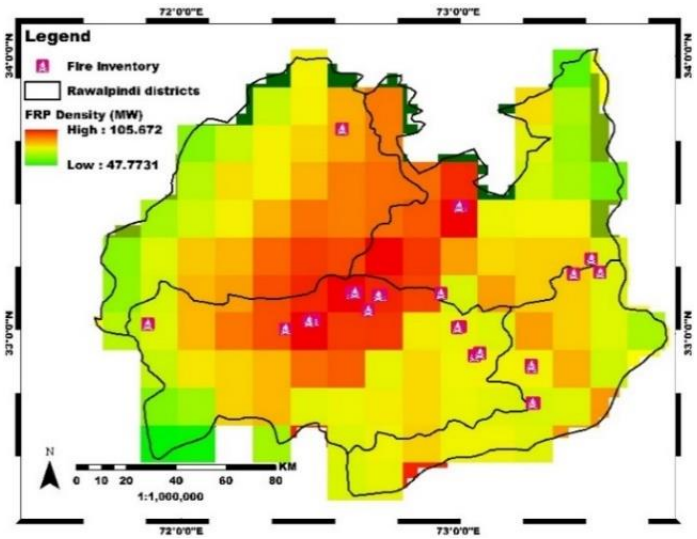

Figure 8. Fire radiative production (FRP) map of Rawalpindi division

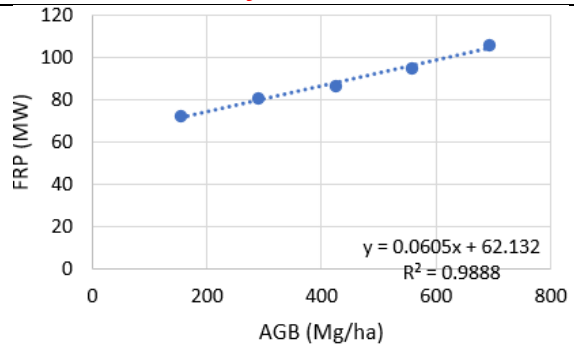

Figure 9. Correlation between FRP and AGB

Even though the procedure is difficult and complex, biomass burned areas can be accurately measured from remotely detected burn scars and ongoing fires. The region damaged by a fire occurrence is known as the "burn scar," and it can be determined by comparing the changes in the vegetation index and spectral reflectance before and after the fire [24]. The burned areas in this study were generally estimated from the interpolation technique (IDW), which displays (Figure 10) the very high, high, moderate, low, and very low area coverage and varied in size from 23.8572, 21.4778, 20.4759, 19.2235, to 14.9656 %.

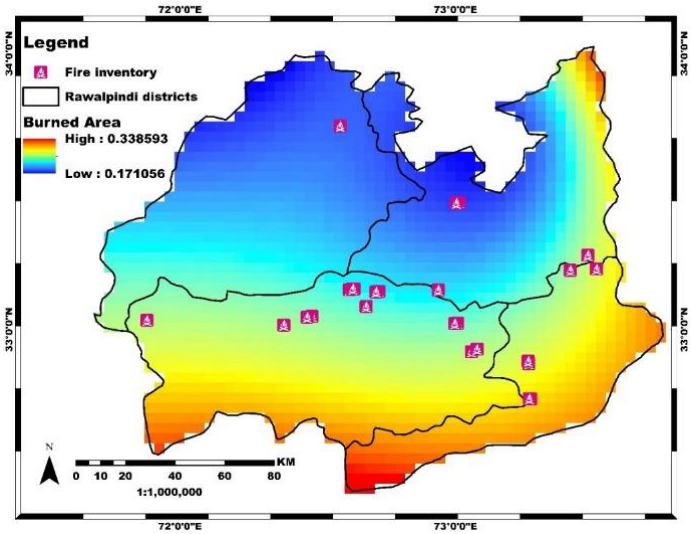

Figure 10. Burned area map of Rawalpindi division

Above Ground Biomass (AGB):

Tropical Forest Biomass:

An essential part of the global carbon cycle is the carbon stock and biomass found in forests. Therefore, to help international programs like REDD+, precise measurement techniques for AGB are needed. According to earlier research, a variety of inventory techniques, including remote sensing, allometric equations, and destructive sampling, have been used in tropical rainforests to estimate the biomass above ground. The spatial-temporal pattern of AGB as tropical forest biomass shows (Figure 11) that the moderate cover area of tropical biomass in 2018 was 813.82 (42.15%), which decreased to 716.74 (37.11%), the low area of tropical forest biomass in 2018 was 566.52 (29.34%), which also decreased in 2024 to 408.89 (21.17%), and the very low area of tropical forest biomass in 2018 was 261.33 (13.53%), which decreased to 184.79 (9.57%). Additionally, the area covered (Table 3) by the high and very high tropical biomass cover in 2018 was 222.66 (11.53%) and 66.33 (3.43%), which increased to 376.87 (19.51%) and 243.62 (12.61%) in 2024. According to the findings, Rawalpindi's forest vegetation served as a carbon sink from 2018 to 2024. These findings are consistent with results of [25]

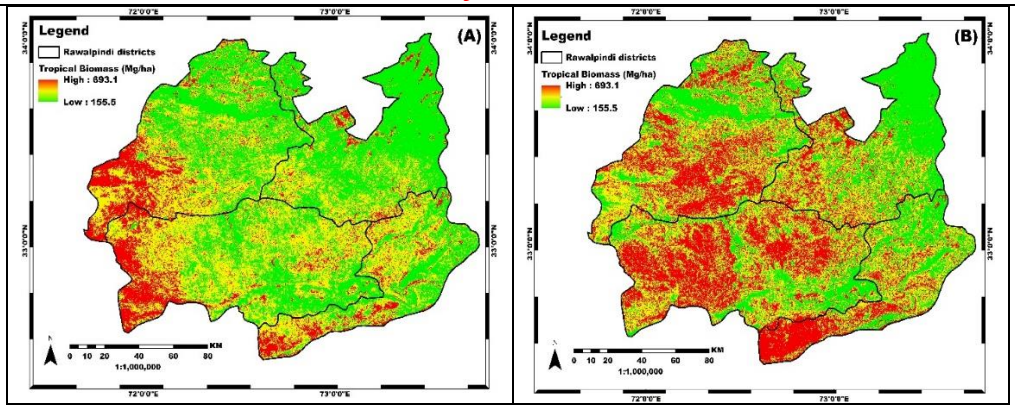

Figure 11. Tropical Forest AGB map of Rawalpindi division (A) 2018 (B) 2024

Table 3. Area calculation of Tropical Forest AGB of Rawalpindi division

Tropical Forest Biomass (Mg/ha)			
2018		2024	
Area (Sqkm)	Area (%)	Area (Sqkm)	Area (%)
261.33	13.5358	184.79	9.5701
566.52	29.3433	408.89	21.176
813.82	42.1524	716.74	37.1193
222.66	11.5328	376.87	19.5177
66.33	3.43561	243.62	12.6168

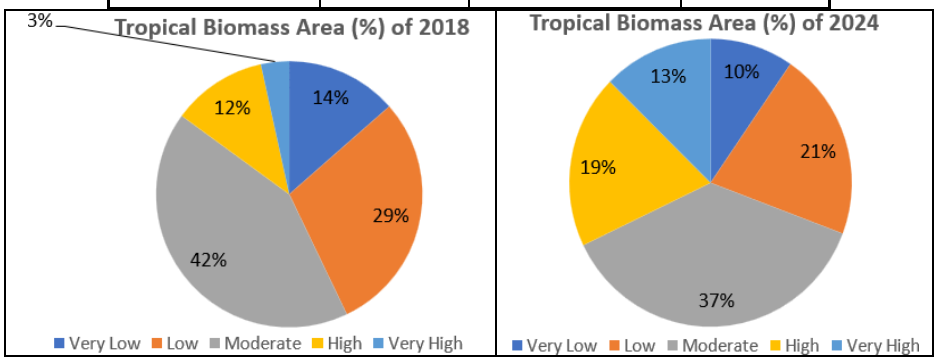

Figure 12. Graphical representation of Tropical Forest AGB area percentage (2018-2024)

Grassland Biomass:

For grassland ecosystems to remain healthy, grassland biomass is necessary[26] The types of grasslands can influence the spatiotemporal patterns of biomass. The dominant plant species can influence the temporal and spatial distribution of biomass in various types of grasslands. Furthermore, the regional distribution and interannual fluctuations of biomass are influenced by environmental factors, including temperature and precipitation. Significant regional heterogeneity was seen in (Figure 13) the biomass distribution, with the biomass rising from the study area's western to eastern sections.

The spatial-temporal pattern of AGB as grassland biomass shows that the moderate cover area of grassland biomass in (Table 4) 2018 was 813.82 sq km (42.15%), which decreased to 716.74 sq km (37.11%), the low area of grassland biomass in 2018 was 566.52 sq km (29.34%), which also decreased in 2024 to 408.89 sq km (21.17%), and the very low area of grassland biomass in 2018 was 261.33 sq km (13.53%), which decreased to 184.79 sq km (9.57%). Additionally, the area covered by the high and very high grassland biomass cover in 2018 was 222.66 sq km (11.53%) and 66.33 sq km (3.43%), which increased to 376.87 sq km (19.51%) and 243.62 sq km (12.61%) in 2024.

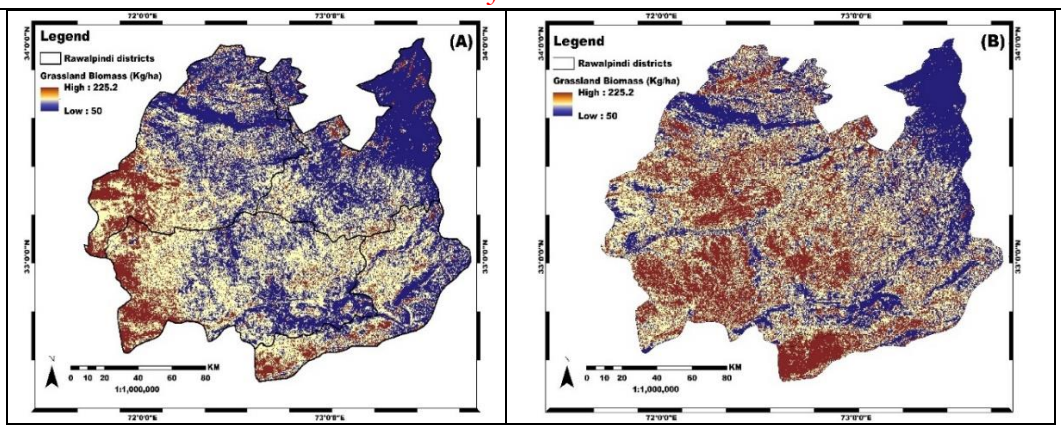

Figure 13. Grassland AGB map of Rawalpindi division (A) 2018 (B) 2024

Table 4. Area calculation of Grassland AGB of Rawalpindi division

Grassland Biomass (kg/ha)			
2018		2024	
Area (Sqkm)	Area (%)	Area (Sqkm)	Area (%)
261.33	13.5358	184.79	9.5701
566.52	29.3433	408.89	21.176
813.82	42.1524	716.74	37.1193
222.66	11.5328	376.87	19.5177
66.33	3.43561	243.62	12.6168

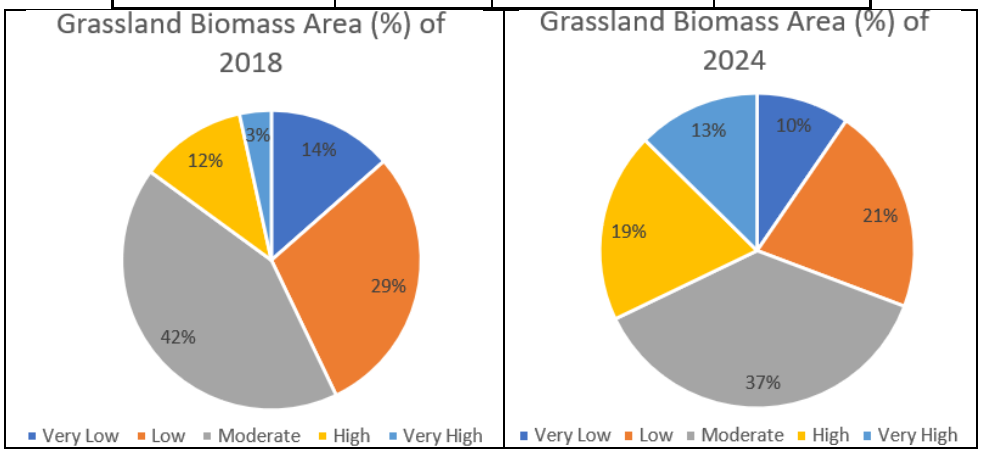

Figure 14. Graphical representation of Grassland AGB area percentage (2018-2024)

Spatial-temporal Variation of Air Pollutants:

Data on carbon stocks and changes in each carbon pool are needed to calculate emission levels. Globally, CO2 emissions are the main contributor to environmental deterioration [10]. A methodology that includes the identification and area estimates of several forest type, biomass carbon, and equivalent CO2 per unit area from each forest type was used to estimate fixed atmospheric CO2 in tree biomass. Carbon fixed by biomass from tree foliage was transformed into equivalent CO2 that was extracted from the atmosphere. Using carbon emissions from the fire zones, we also computed the average carbon emissions in (Figure 15) of forests, shrubs, and grasses, which were 346.55 Mg/ha as high and 77 Mg/ha, respectively, from 2018–2024. The greatest average increases as in (Table 5 and Figure 17) in carbon emissions in the region are produced by forests, which produced 66.33 (3.43%) in 2018 to 243.62 (12.61%), roughly equal to the emissions from grasses and shrubs, respectively. The research region's (Figure 16) estimated carbon stock in 2024 was 82 t/ha, with the lowest area being 1388.12 9 (35.75%). The value of the carbon stock and biomass increased with forest density.

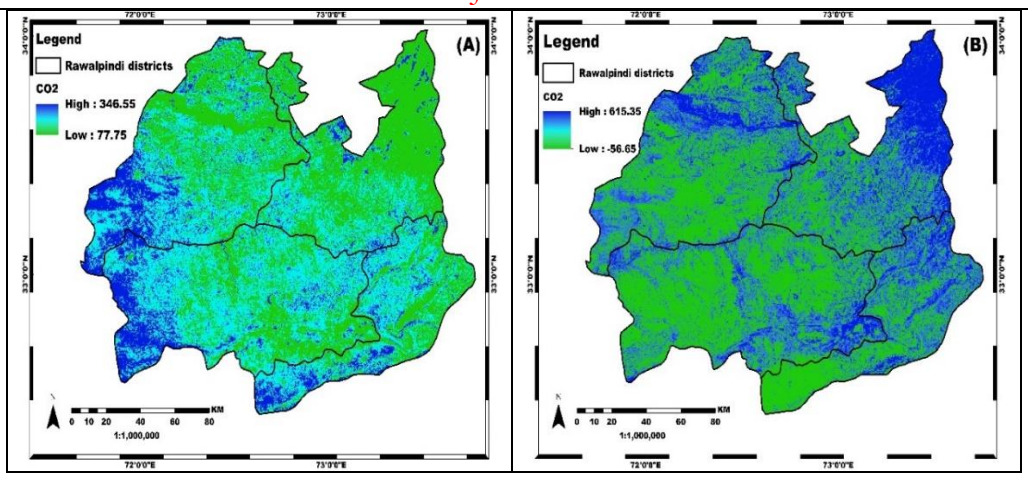

Figure 15. Carbon dioxide (CO_2) map of Rawalpindi division (A) 2018 (B) 2024

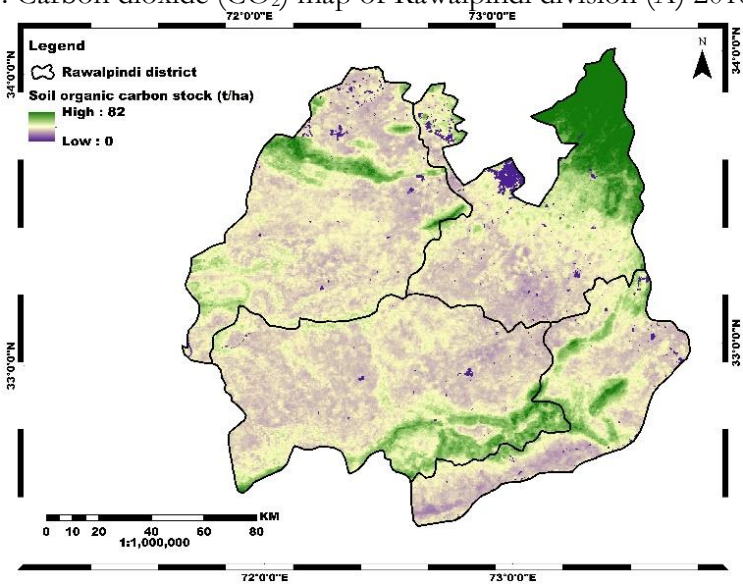

Figure 16. Carbon stock map of Rawalpindi division

Table 5. Area calculation of Carbon dioxide (CO_2) emission of Rawalpindi division

CO_2 Emission			
2018		2024	
Area (Sqkm)	Area (%)	Area (Sqkm)	Area (%)
261.33	13.5358	184.79	9.5701
566.52	29.3433	408.89	21.176
813.82	42.1524	716.74	37.1193
222.66	11.5328	376.87	19.5177
66.33	3.43561	243.62	12.6168

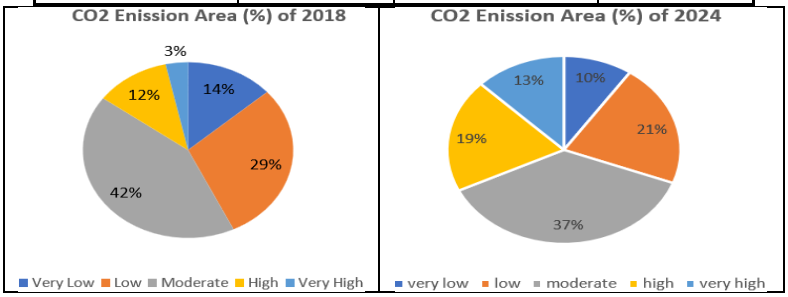

Figure 17. Graphical representation of Carbon dioxide (CO_2) emission area percentage (2018-2024)

The total emissions from forest fires and agricultural waste residues from 2018–2024 were calculated using Equation (1) for the forest area and Equation (2) for agricultural leftovers to evaluate the air emissions from open biomass burning. The (Figure 18) results show that air pollutants from forest fires in 2018 ranged from 0.000008557 (mol/m^2) to 0.000218619 (mol/m^2), whereas the range of NO2 in 2024 was between 0.00002336 (mol/m^2) and 0.000066323 (mol/m^2). The lowest NO2 emission area in 2018 was 220.08 (41.15%), which has since dropped to 98.38 (18.37%), while the maximum coverage area (Table 6) was 10.81 (2.021%), which has already risen to 25.92 (4.84%) in 2024.

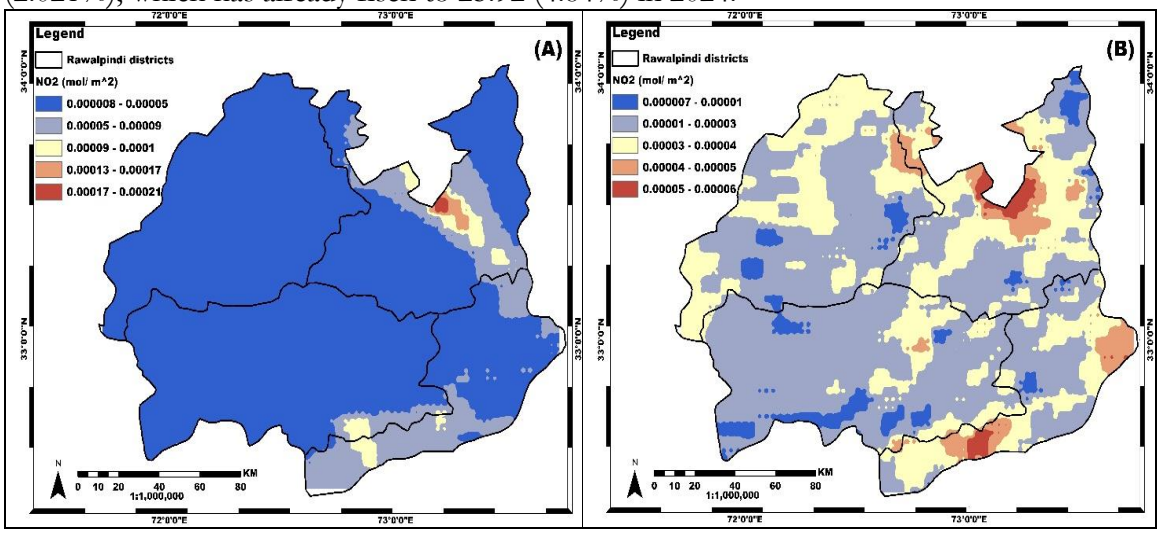

Figure 18. Nitrogen dioxide (NO_2) map of Rawalpindi division (A) 2018 (B) 2024

Table 6. Area calculation of Nitrogen dioxide (NO_2) emission of Rawalpindi division

NO2 Emission			
2018		2024	
Area (Sqkm)	Area (%)	Area (Sqkm)	Area (%)
220.08	41.1534	98.38	18.3754
178.61	33.3988	192.87	36.0242
87.53	16.3675	136.93	25.5757
37.75	7.05898	81.29	15.1833
10.81	2.02139	25.92	4.84133

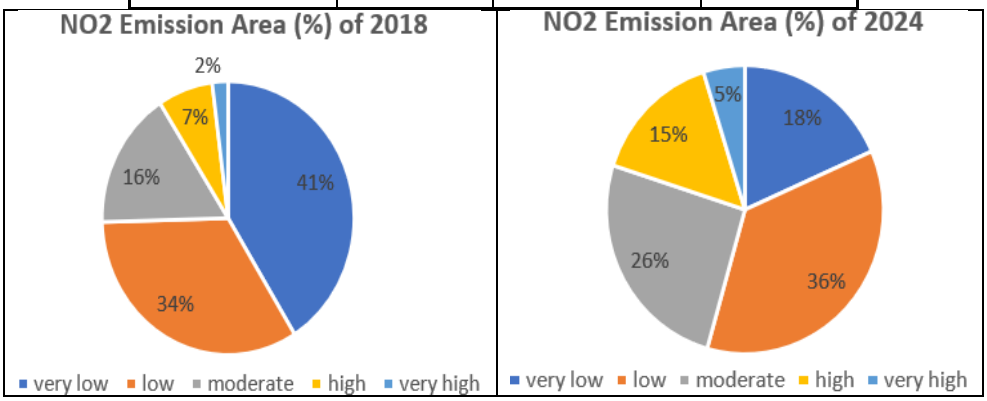

Figure 19. Graphical representation of Nitrogen dioxide (NO_2) emission area percentage (2018-2024)

Notably, the (Figure 20) emissions in 2018 ranged from -0.000409846 (mol/m²) to 0.000981901 (mol/m²) of SO_2, while the concentration level of emissions in 2024 was from -0.000314715 (mol/m²) to 0.001403507 (mol/m²). The highest area of SO_2 (Table 7) emissions in 2018 was 4.99 sq km (14.62%), which has since decreased to 3.88 sq km (11.36%), and the

lowest concentration level area of SO_2 emissions was 2.36 sq km (6.91%) in 2018, while the lowest emission level area has increased to 2.41 sq km (7.06%)

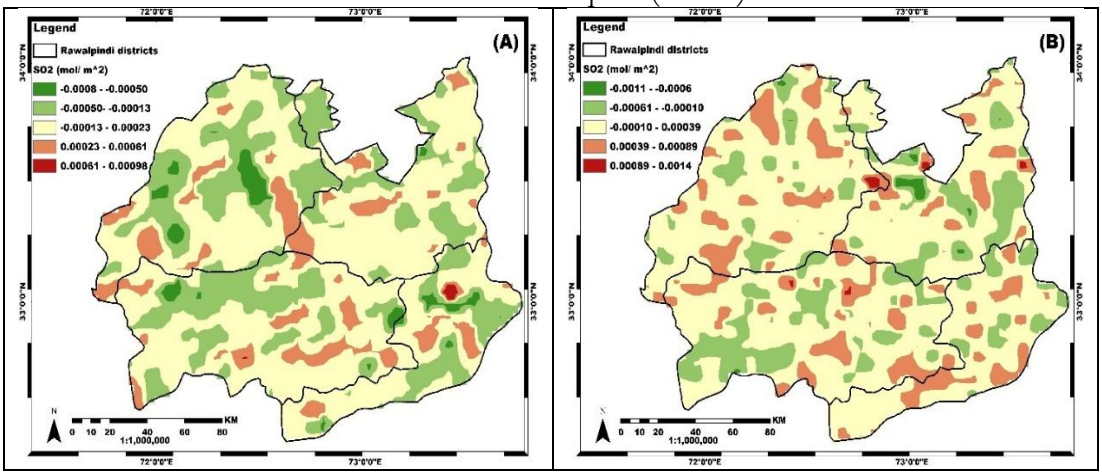

Figure 20. Sulphur dioxide (SO_2) map of Rawalpindi division (A) 2018 (B) 2024

Table 7. Area calculation of Sulphur dioxide (SO_2) emission of Rawalpindi division

SO2 Emission			
2018		2024	
Area (Sqkm)	Area (%)	Area (Sqkm)	Area (%)
2.36	6.91474	2.41	7.06124
6.68	19.5722	7.19	21.0665
9.11	26.6921	11.64	34.1049
10.99	32.2004	9.01	26.3991
4.99	14.6206	3.88	11.3683

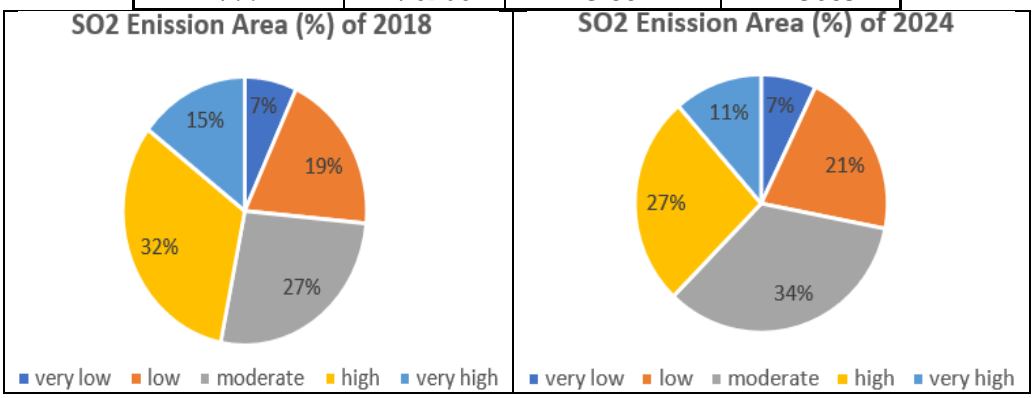

Figure 21. Graphical representation of Sulphur dioxide (SO_2) emission area percentage (2018-2024)

Aerosol emission (Figures 22 and 23) values range from 0.44 (mol/m²) to 1.92 (mol/m²), with the maximum area being 2.71 sq km (7.99%) and the lowest being 4.34 sq km (12.8%). The maximum area coverage of aerosols in the atmosphere was 4.47 sq km (13.18%), while the lowest area was 7.89 sq km (23.10%). In contrast (Table 8), the lowest to highest air emissions were recorded in 2024, ranging from -1.614 (mol/m²) to 0.099 (mol/m²) of aerosol. The comparison map makes the steady rise in aerosol emissions in Rawalpindi Division quite evident.

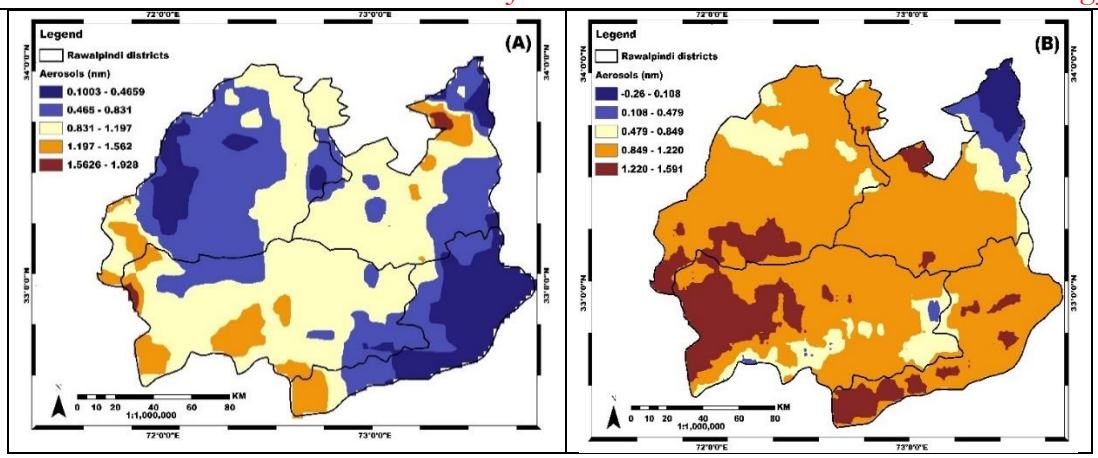

Figure 22. Aerosol's map of Rawalpindi division (A) 2018 (B) 2024

Table 8. Area calculation of Aerosol's emission of Rawalpindi division (2018-2024)

Aerosol Emission			
2018		2024	
Area (Sqkm)	Area (%)	Area (Sqkm)	Area (%)
4.34	12.8024	7.89	23.104
8.15	24.0413	6.77	19.8243
9.69	28.5841	7.93	23.2211
9.01	26.5782	7.09	20.7613
2.71	7.9941	4.47	13.0893

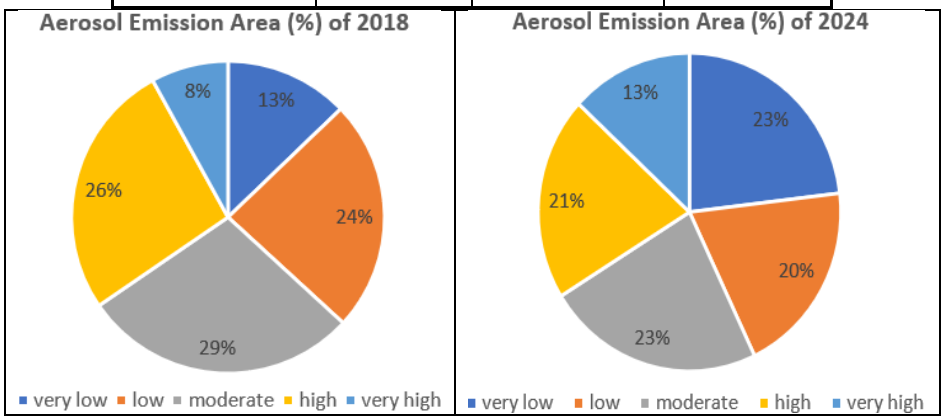

Figure 23. Graphical representation of Aerosol's emission area percentage (2018-2024)

Carbon monoxide (CO) concentrations (Figure 24) ranged from 0.031 (mol/m²) to 0.045 (mol/m²) in 2018, whereas 2024 emission levels ranged from 0.032 (mol/m²) to 0.042 (mol/m²). The lowest CO emission area (Figure 25) in 2018 was 8.33 sq km (1.55%), which rose to 84.18 sq km (15.72%) in 2024. In 2018, the greatest CO emission area (Table 9) was 48.4 sq km (9.05%), which increased to 66.37 sq km (12.39%).

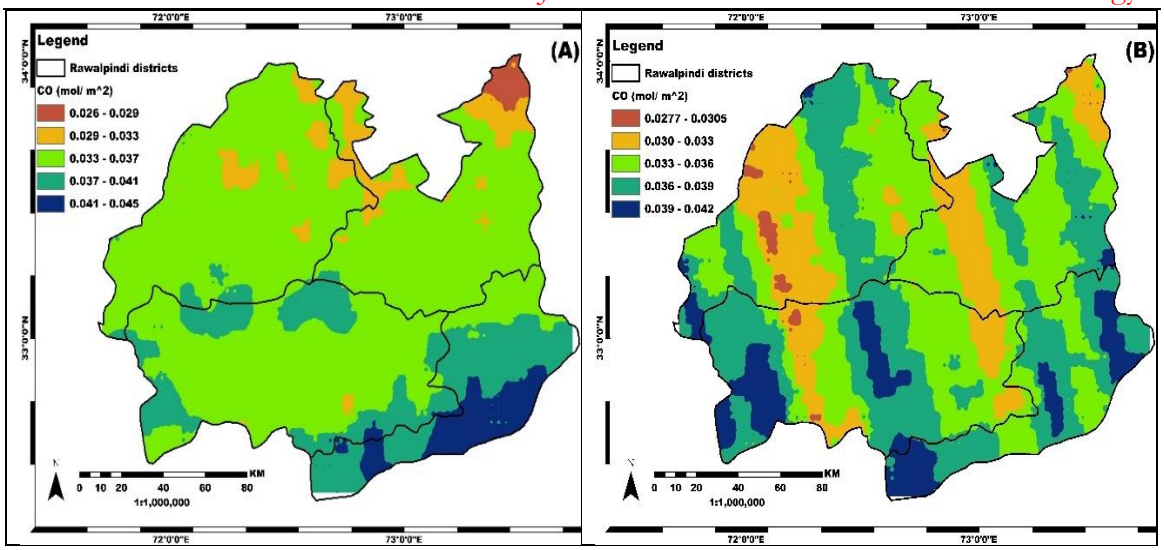

Figure 24. Carbon monoxide (CO) map of Rawalpindi division (A) 2018 (B) 2024

Table 9. Area calculation of Carbon monoxide (CO) emission of Rawalpindi division (2018-2024)

CO Emission			
2018		2024	
Area (Sqkm)	Area (%)	Area (Sqkm)	Area (%)
8.33	1.55765	84.18	15.7231
145.48	27.2037	110.44	20.628
224.38	41.9574	149	27.8302
108.19	20.2307	125.4	23.4222
48.4	9.05045	66.37	12.3966

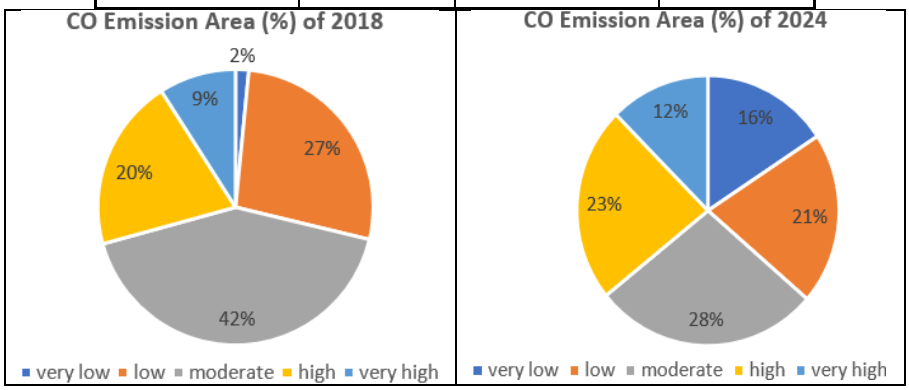

Figure 25. Graphical representation of Carbon monoxide (CO) emission area percentage (2018-2024)

Ozone (O_3) concentrations (Figure 26) in 2018 ranged from low to high, from 0.129 (mol/m²) to 0.134 (mol/m²). In contrast, O_3 concentrations in 2024 ranged from 0.128 (mol/m²) to 0.134 (mol/m²). In (Figure 27) 2018, the ozone cover of the atmosphere was at its lowest, measuring 2.57 sq km (7.51%), and it grew to 7.2 sq km (21.05%) in 2024. In contrast (Table 10), the maximum area of ozone concentration in 2018 was 5.6 sq km (16.37%), but it decreased to 4.05 sq km (11.84%) in 2024.

Table 10. Area calculation of Ozone (O_3) emission of Rawalpindi division (2018-2024)

O3 Emission			
2018		2024	
Area (Sqkm)	Area (%)	Area (Sqkm)	Area (%)
2.57	7.51462	7.2	21.0526

5.5	16.0819	8.17	23.8889
9.86	28.8304	7.37	21.5497
10.67	31.1988	7.41	21.6667
5.6	16.3743	4.05	11.8421

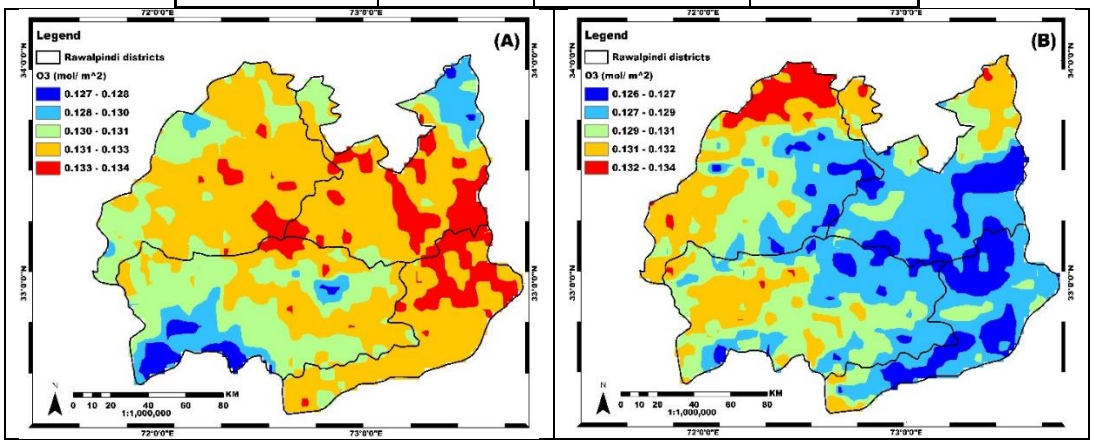

Figure 26. Ozone (O_3) map of Rawalpindi division (A) 2018 (B) 2024

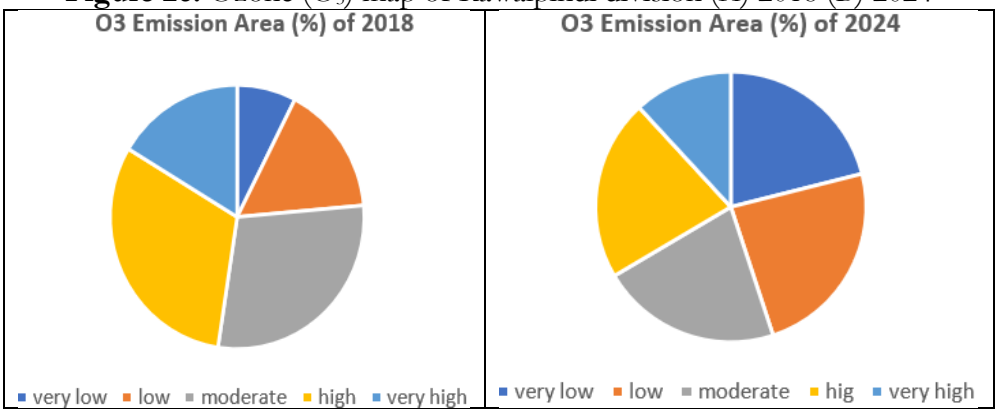

Figure 27. Graphical representation of Ozone (O_3) emission area percentage (2018-2024)

Pearson Correlation Between Biomass and Influencing Factors:

Vegetation and AGB:

According to the research findings (Figures 28 and 29), the AGB of forests and the reported NDVI showed a positive correlation in 2018 (R^2=0.82) and 2024 (R^2=0.89). In 2018, there was a direct association between vegetation biomass, which was calculated using the grassland biomass equation (kg/ha), and vegetation indices (NDVI), with a correlation of R^2=0.8166; however, in 2024, the correlation between AGB for grassland and NDVI was R^2=0.8901. NDVI is a vegetation index that was significantly ($p < 0.01$) correlated with biomass, according to the graphs.

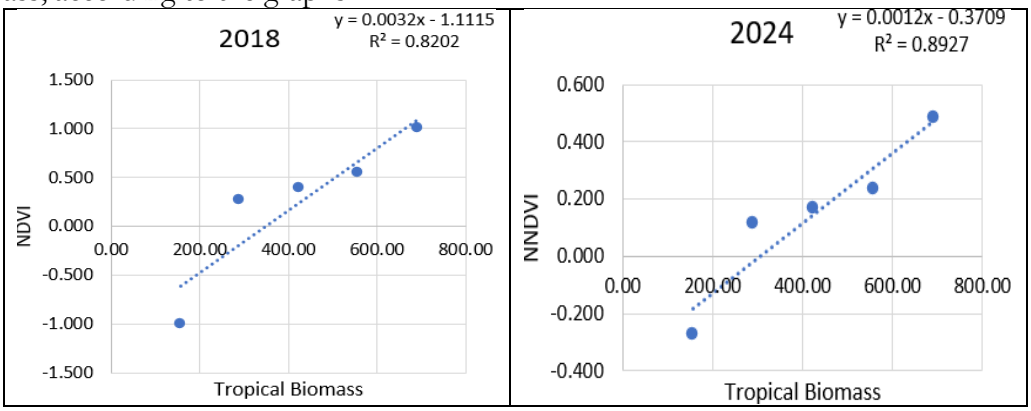

Figure28. Correlation between tropical forest AGB and NDVI (2018-2024)

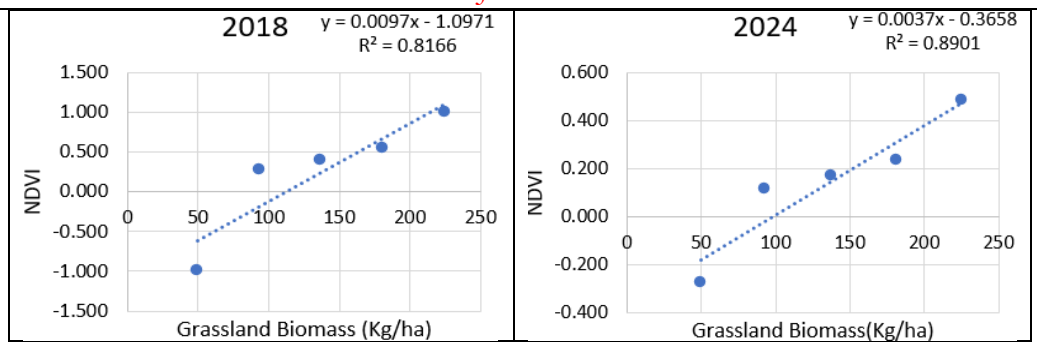

Figure 29. Correlation between Grassland AGB and NDVI (2018-2024)

LST and AGB:

The physical connections between shortwave and thermal data are the foundation of both downscaling strategies. The most significant of them is the relationship between the LST and biomass levels, which may be determined using indices like the NDVI or shortwave reflectance. Each variable's graph against AGB demonstrates the increasing linear relationship between LST and AGB. However, as AGB grew, the NDVI tended to decline over time after initially showing an increasing connection. The "Longitude, Latitude" interaction revealed a correlation between Rawalpindi's northern and western forests and regions with higher AGB. Meanwhile, regions with lower LST have higher levels of AGB. Finally, in regions (Figures 30 and 31) with lower elevation and temperatures, the "LST, DEM" interaction demonstrated a positive correlation with AGB. In 2018, there was a positive association between AGB and LST for the tropical forest (R^2 = 0.98), and the direct relationship was linear (R^2 = 0.96). However, the findings show that there is a positive association between AGB and grassland in 2018 (R^2 = 0.9866), whereas in 2024 (R^2 = 0.9646), there is a positive correlation.

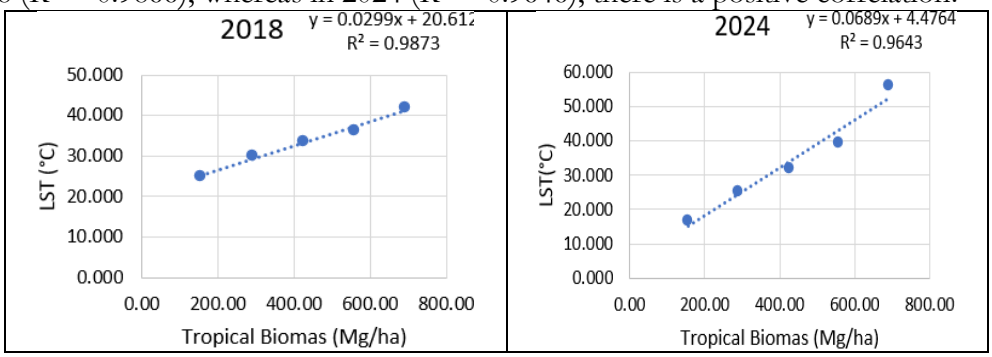

Figure 30. Correlation between tropical forest AGB and LST (2018-2024)

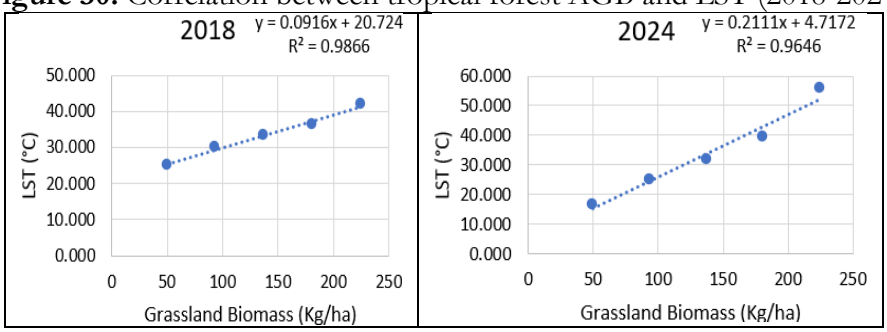

Figure 31 Correlation between Grassland AGB and LST (2018-2024)

Carbon Stock and AGB:

According to the Intergovernmental Panel on Climate Change (IPCC) United Nations Programme, carbon reserves in forest ecosystems are mainly found in the following locations: above-ground biomass (AGB), below-ground biomass, forest litter layer, woody debris, and organic matter in soil. Total ecosystem carbon stocks in the soil, litter layer, and tree biomass

in 34-year-old plantations were significantly greater in the forest in the northwestern highlands of Punjab Province, Rawalpindi Division. The (Figure 32) relationship between total carbon stock in the ecosystem of the study area was positively correlated ($R^2 = 0.9275$)

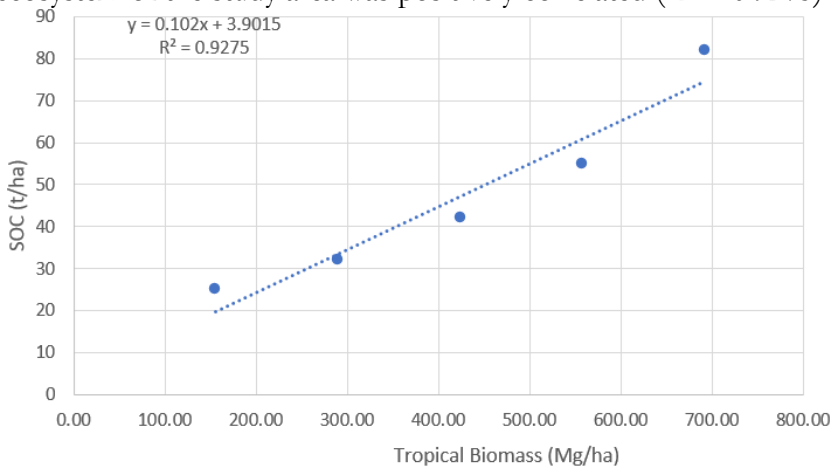

Figure 32. Correlation between tropical forest AGB and carbon stock

Relationship between Air pollutants and Biomass:

Carbon Dioxide (CO_2) and AGB:

(Figures 33 and 34) findings from 2018 indicate that there is a positive association ($R^2 = 1$) between the AGB for forests and the grassland AGB. Conversely, the 2024 data reveal a linear trend indicating a positive relationship ($R^2 = 0.9242$) between CO_2 and tropical forest biomass, and an estimated association ($R^2 = 0.9239$) between CO_2 and grassland AGB.

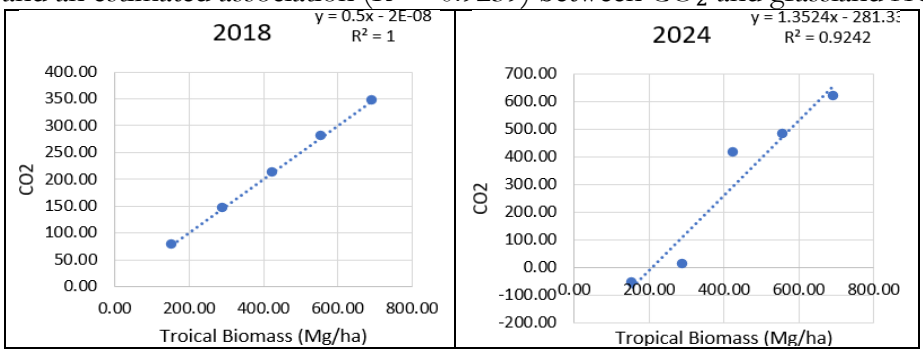

Figure33. Correlation between tropical forest AGB and CO_2 (2018-2024)

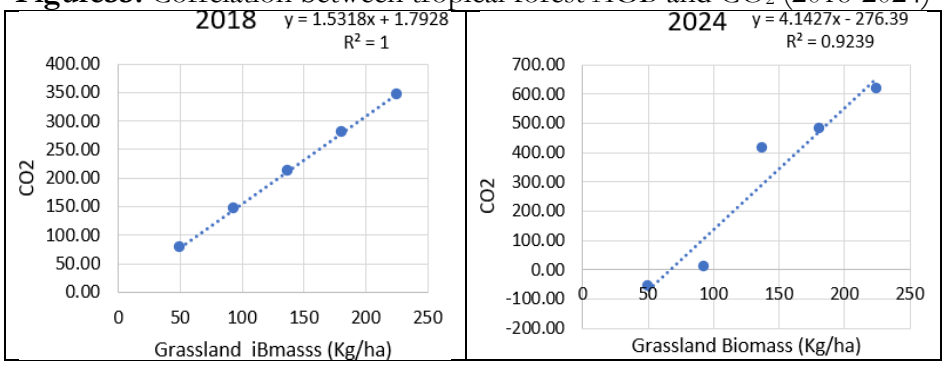

Figure 34. Correlation between Grassland AGB and CO_2 (2018-2024**)**

Carbon monoxide and AGB:

[27] stated that when carbon monoxide (CO) is present in ambient air in high amounts, it can have detrimental effects on health, particularly on the respiratory system. The following CO concentrations on a city scale and the identification of high-concentration locations with a single overpass have been made possible using the TROPOMI instrument. The (Figures 35 and 36) findings of the correlation study between CO levels and other climate variables for

Rawalpindi cities are shown in Figure 6 for each of the years 2018–2024. Throughout the entire study period, the CO measurement and AGB for tropical forest biomass showed a positive correlation in 2018 (R^2 = 0.9676); in contrast, the 2024 data indicate a value of (R^2 = 0.9818). Throughout the entire study period, the CO measurement and AGB for grassland biomass showed a positive correlation in 2018 (R^2 = 0.9679); however, in 2024, there was a positive correlation (R^2 = 0.9822).

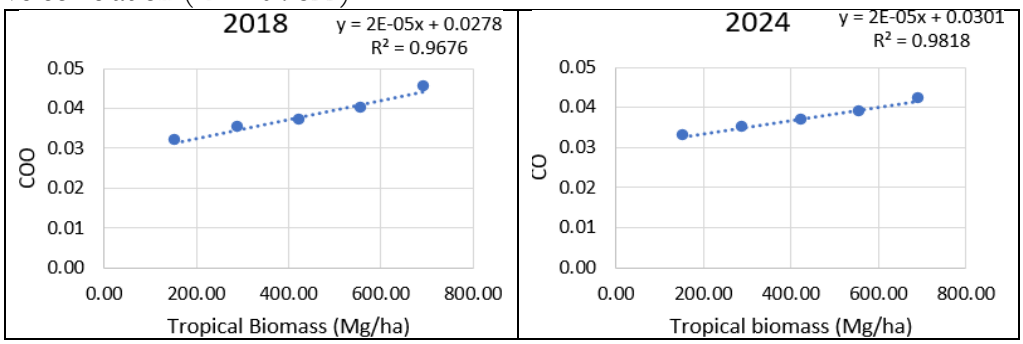

Figure 35. Correlation between tropical forest AGB and CO (2018-2024)

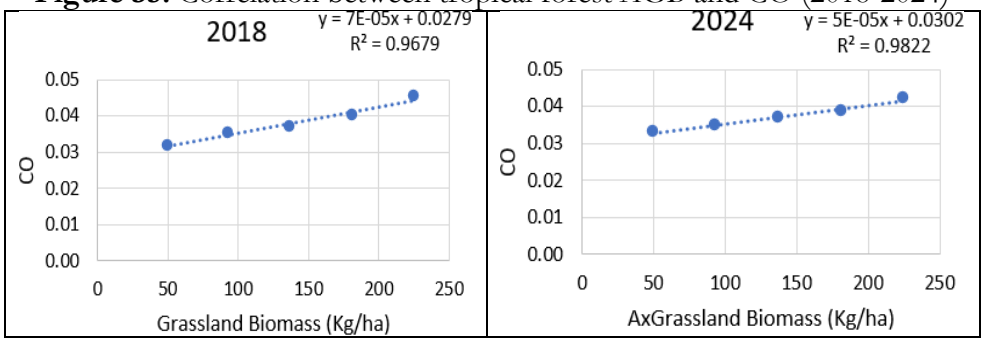

Figure 36. Correlation between Grassland AGB and CO (2018-2024)

NO_2 and AGB:

Our findings (Figures 37 and 38) regarding the NO_2 gas monitoring over the Rawalpindi Division show significant differences between the time frames of the 2018 and 2024 periods from June 1 to September 30. The p-value, which evaluated the correlation significance level, yielded values below 5% for every scenario that was encountered, demonstrating the significance of the correlations. In the six years between 2018 and 2024, the Pearson correlation coefficient between tropical forest AGB and NO_2 yielded values ranging from 0.597 to 0.865, indicating that all correlations are positively linear. In 2018, the Pearson linear correlation between grassland biomass and NO_2 was R^2 = 0.9097. However, in 2024, the estimated results reveal a positive correlation of R^2 = 0.8601.

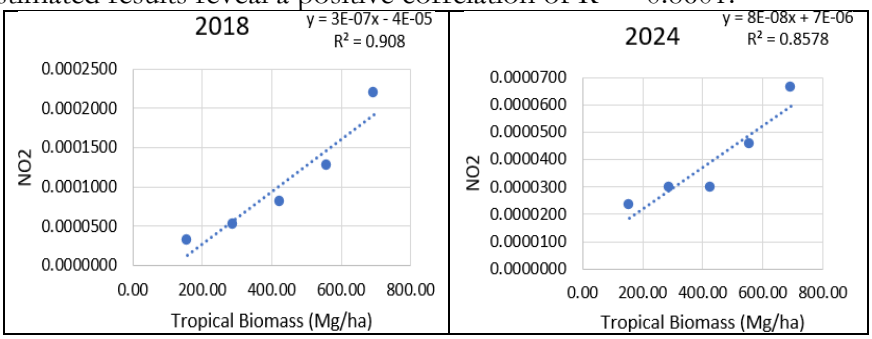

Figure 37. Correlation between tropical forest AGB and NO_2 (2018-2024)

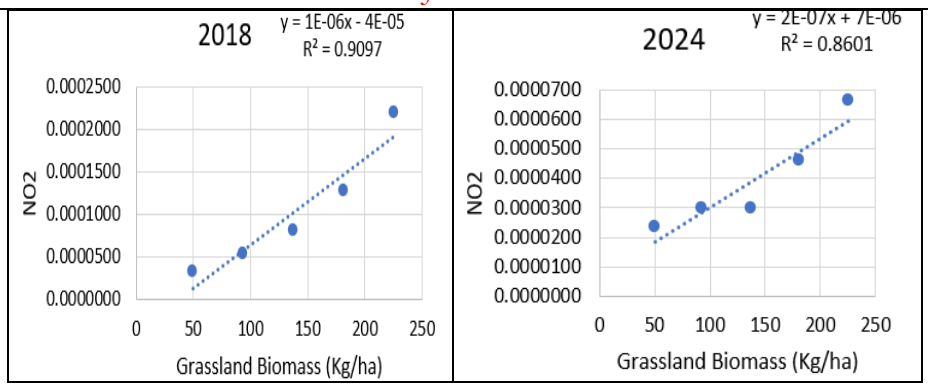

Figure 38. Correlation between Grassland AGB and NO_2 (2018-2024)

SO_2 and AGB:

Variability in coal content, power generation plant design, coal-fired plant location, and ambient temperature-related air conditions could all contribute to the spatial and temporal variability seen in SO_2 emissions results. The graph (Figures 39 and 40) displays the Rawalpindi region's SO_2 linear regression trends. Over time, a notable upward trend in SO_2 is noted. Additionally, the Pearson linear regression indicates a rising trend in SO_2 between 2018 and 2024. In 2018 and 2024, there was a positive correlation between AGB for tropical forests and SO_2 ($R^2 = 0.8876$ and $R^2 = 0.8971$, respectively). However, the results of the 2018 correlation study show that $R^2 = 0.8885$, while the 2024 analysis shows that grassland AGB and SO_2 have a positive correlation of $R^2 = 0.8979$.

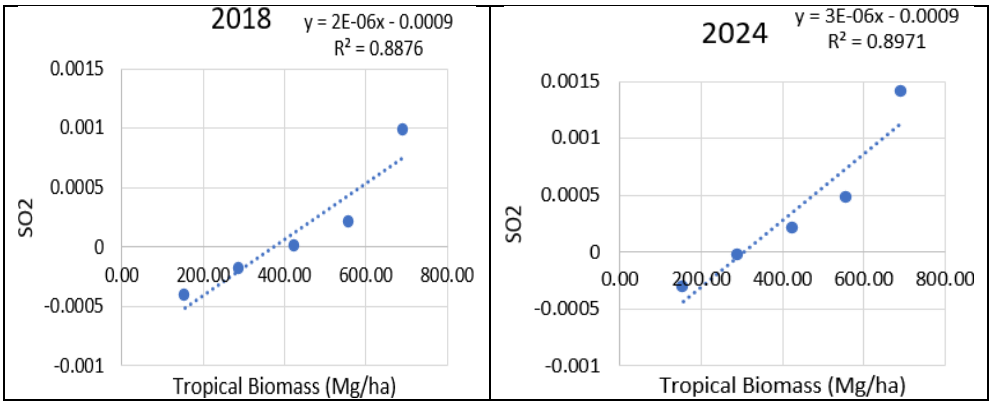

Figure 39. Correlation between tropical forest AGB and SO_2 (2018-2024)

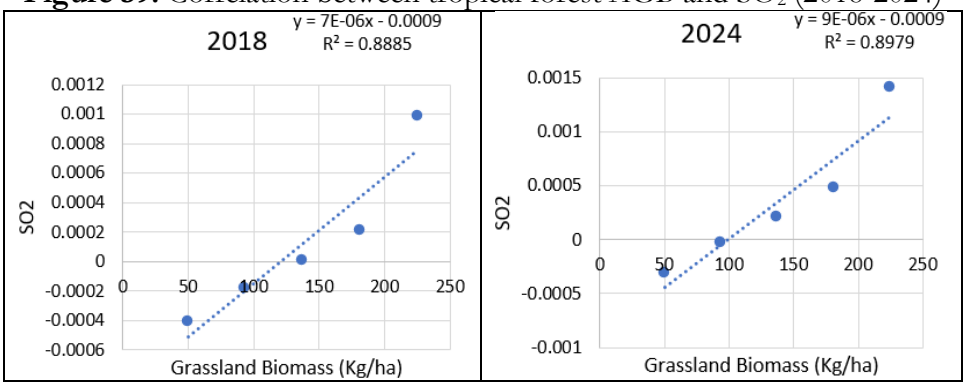

Figure 40. Correlation between Grassland AGB and SO_2 (2018-2024)

Aerosol and AGB:

Emissions from burning biomass alter the composition of the atmosphere and the characteristics of aerosols. Burning biomass alters the composition of the atmosphere and the characteristics of aerosols, highlighting the intricate interactions between these variables [28] (Figures 41 and 42) Regression analysis in 2018 revealed a positive correlation ($R^2 = 0.937$)

between aerosol and AGB for forests, whereas the results for 2024 showed a positive linear regression ($R^2 = 0.9156$). Regression analysis in 2024 shows a correlation of $R^2 = 0.9165$, while positive linear analysis between aerosol and grassland biomass (AGB) shows $R^2 = 0.9377$ in 2018.

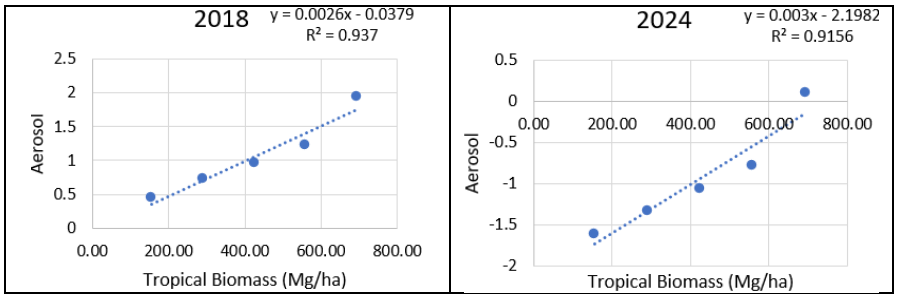

Figure 41. Correlation between tropical forest AGB and aerosols (2018-2024)

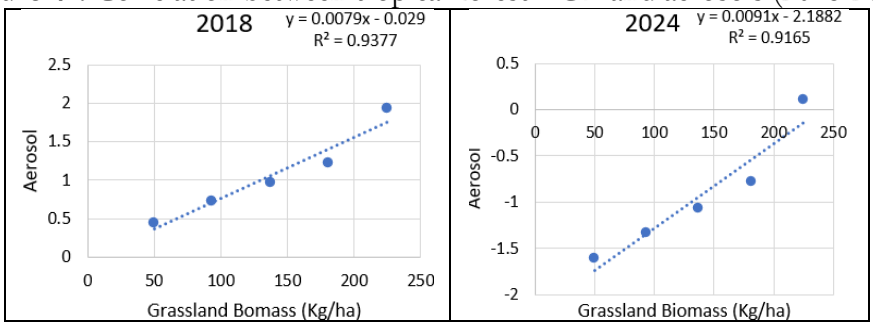

Figure42. Correlation between Grassland AGB and aerosols (2018-2024)

O3 and AGB:

The most phytotoxic air pollutant for vegetation may be ground-level ozone (O_3). Without the interaction between O_3 and species, there were notable changes in leaf biomass and the root/shoot ratio between species [29] A relationship between O_3 and above-ground biomass (AGB) was assessed using a regression analysis for 2018 and 2024. (Figures 43 and 44) In contrast, the 2024 analysis reveals a linear correlation of $R^2 = 0.972$ between tropical forest biomass and O_3, and the 2018 results show a positive correlation of $R^2 = 0.9879$. In 2018, there was a positive linear regression between grassland biomass and O_3 ($R^2 = 0.9874$); however, in 2024, there was a positive correlation ($R^2 = 0.9727$).

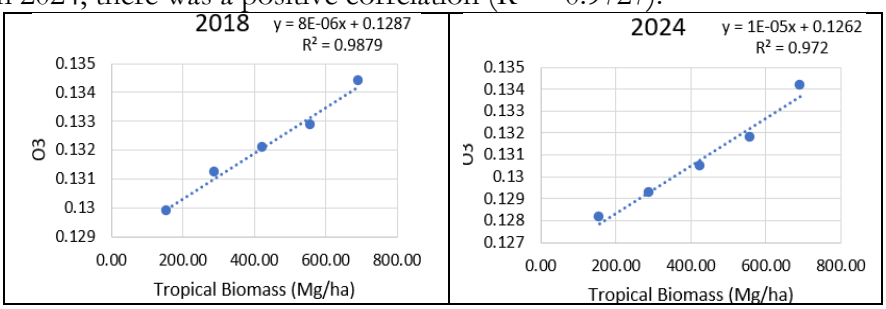

Figure 43. Correlation between tropical forest AGB and O_3 (2018-2024)

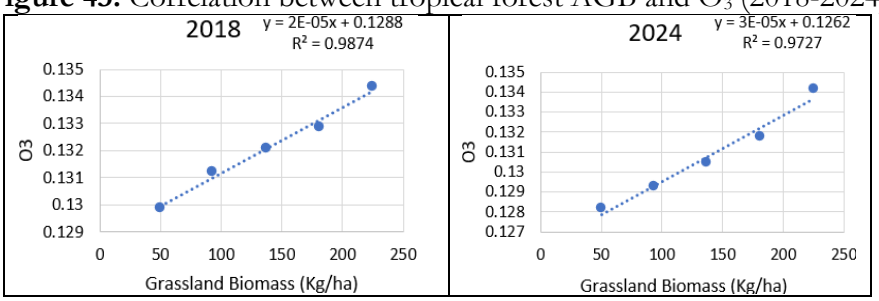

Figure 44. Correlation between Grassland AGB and O_3 (2018-2024)

Conclusion:

Biomass burning due to forest fires and agricultural waste burning has been a major concern in Southeast Asia, affecting human health, atmospheric visibility, land use, and aquatic ecosystems. Burning biomass has complicated effects on the climate that vary by time, space, and fire intensity. Burning biomass releases a variety of gases and aerosols into the atmosphere that affect the Earth's radiative budget, global atmospheric chemistry, biogeochemical cycles, visibility, regional air quality, and climate change. In this study, we used the Multiscale Air Quality Index and the influence of fire activity due to biomass burning emission inventory to simulate biomass burning in the Rawalpindi Division from June to July of 2018–2024. The use of agricultural lands is correlated with the trend of air emissions, with sugarcane plantations having the highest emissions, followed by corn plantations, forest areas, and rice plantations, in that order. In this study, we examined the spatial-temporal variation of AGB from vegetation for forest cover and grassland in Rawalpindi using the Sentinel-2, Sentinel-3, and Sentinel-5P combination. We also evaluated the effects of burning biomass on air quality by measuring the amount of greenhouse gases released into the Rawalpindi region's atmosphere. The findings show that above-ground biomass (AGB) increased gradually between 2018 and 2024, with an unstable emission trend that began in 2018 and ended in 2024 with a peak. The La Niña phenomenon and climate change are two factors that contribute to this volatility. In the La Niña years of 2018 and 2024, temperatures rose significantly during normally dry seasons, causing fuel moisture levels to deviate from normal. The estimation of the land surface temperature (LST°C), emissions from burning biomass, and the types of pollutants (mol/m²), such as NO_2, SO_2, CO, and O_3 aerosols, as well as the spatial-temporal distribution of vegetation cover (NDVI) from 2018 to 2024. Pearson correlation has been used to assess the relationship between tropical forest biomass and grassland biomass with all influencing factors, including air pollutants, meteorological parameters like temperature, and fire radiative power (FRP). The results show that FRP values are 72.067, 80.46, 86.372, 94.54, and 105.67. The increasing tendency of biomass in the study region is shown by the positive correlation with the linear trend. Furthermore, stakeholders can use the AGB estimates produced using the proposed methodology for forest management plans and carbon trade policies.

References:

[1] M. H. Sawar Khan, Ayesha Nisar, Bo Wu, Qi-Li Zhu, Yan-Wei Wang, Guo-Quan Hu, "Bioenergy production in Pakistan: Potential, progress, and prospect," *Sci. Total Environ.*, vol. 814, p. 152872, 2022, doi: https://doi.org/10.1016/j.scitotenv.2021.152872.

[2] D. Lu, Q. Chen, G. Wang, L. Liu, G. Li, and E. Moran, "A survey of remote sensing-based aboveground biomass estimation methods in forest ecosystems," *Int. J. Digit. Earth*, vol. 9, no. 1, pp. 63–105, 2016, doi: 10.1080/17538947.2014.990526.

[3] H. S. Fugen Jiang, Mykola Kutia, Kaisen Ma, Song Chen, Jiangping Long, "Estimating the aboveground biomass of coniferous forest in Northeast China using spectral variables, land surface temperature and soil moisture," *Sci. Total Environ.*, vol. 785, p. 147335, 2021, doi: https://doi.org/10.1016/j.scitotenv.2021.147335.

[4] H. Temesgen, D. Affleck, K. Poudel, A. Gray, and J. Sessions, "A review of the challenges and opportunities in estimating above ground forest biomass using tree-level models," *Scand. J. For. Res.*, vol. 30, no. 4, pp. 326–335, May 2015, doi: 10.1080/02827581.2015.1012114.

[5] Y. P. Mtui, "Tropical rainforest above ground biomass and carbon stock estimation for upper and lower canopies using terrestrial laser scanner and canopy height model from unmanned aerial vehicle (UAV) imagery in Ayer-Hitam, Malaysia," *Univ. Twente*, 2017, [Online]. Available: http://essay.utwente.nl/83598/1/mtui.pdf

[6] Mauro Bologna & Gerardo Aquino, "Deforestation and world population

sustainability: a quantitative analysis," *Sci. Rep.*, 2020, [Online]. Available: https://www.nature.com/articles/s41598-020-63657-6

[7] Y. F. L. Kan Huang, Joshua S. Fu a, N. Christina Hsu, Yang Gao, Xinyi Dong, Si-Chee Tsay, "Impact assessment of biomass burning on air quality in Southeast and East Asia during BASE-ASIA," *Atmos. Environ.*, vol. 78, pp. 291–302, 2013, doi: https://doi.org/10.1016/j.atmosenv.2012.03.048.

[8] H. Mahmood, "Trade, FDI, and CO2 emissions nexus in Latin America: the spatial analysis in testing the pollution haven and the EKC hypotheses," *Environ. Sci. Pollut. Res.*, vol. 30, no. 6, pp. 14439–14454, Feb. 2023, doi: 10.1007/S11356-022-23154-X/METRICS.

[9] H. K. Lirong Cai, "Global models and predictions of plant diversity based on advanced machine learning techniques," *New Phytol.*, 2023, [Online]. Available: https://nph.onlinelibrary.wiley.com/doi/10.1111/nph.18533

[10] M. N. Syed Rashid Ali, "Sectoral carbon dioxide emissions and environmental sustainability in Pakistan," *Environ. Sustain. Indic.*, vol. 23, p. 100448, 2024, doi: https://doi.org/10.1016/j.indic.2024.100448.

[11] "World Energy Outlook 2023 – Analysis - IEA." Accessed: Jul. 31, 2025. [Online]. Available: https://www.iea.org/reports/world-energy-outlook-2023

[12] M. Qasim, S. Ahmad, and A. Shoukat, "World Adoption of Renewable Energy and the Role of Pakistan in Green Energy Production," *ICT-PEP 2022 - Int. Conf. Technol. Policy Energy Electr. Power Adv. Technol. Transitioning to Sustain. Energy Mod. Power Syst. Proc.*, pp. 139–144, 2022, doi: 10.1109/ICT-PEP57242.2022.9988934.

[13] R. S. C. M. Diego Marcelino do Nascimento, Aldo Torres Sales, Rodolfo Souza, Antonio Samuel Alves da Silva, Everardo Valadares de Sa Barretto Sampaio, "Development of a methodological approach to estimate vegetation biomass using remote sensing in the Brazilian semiarid NE region," *Remote Sens. Appl. Soc. Environ.*, vol. 27, p. 100771, 2022, doi: https://doi.org/10.1016/j.rsase.2022.100771.

[14] D. Z. Georgia Galidaki, "Vegetation biomass estimation with remote sensing: focus on forest and other wooded land over the Mediterranean ecosystem," *Int. J. Remote Sens.*, vol. 38, no. 7, 2017, [Online]. Available: https://www.tandfonline.com/doi/full/10.1080/01431161.2016.1266113

[15] A. U. R. R. Bilal Muhammad, "Estimation of above-ground biomass in dry temperate forests using Sentinel-2 data and random forest: a case study of the Swat area of Pakistan," *Front. Environ. Sci*, vol. 12, 2024, doi: https://doi.org/10.3389/fenvs.2024.1448648.

[16] "Brief on Census -2017 | Pakistan Bureau of Statistics." Accessed: Jul. 01, 2024. [Online]. Available: https://www.pbs.gov.pk/content/brief-census-2017

[17] P. M. L.-S. Marcela Rosas-Chavoya, "Estimating Above-Ground Biomass from Land Surface Temperature and Evapotranspiration Data at the Temperate Forests of Durango, Mexico," *Forests*, vol. 14, no. 2, 2023, doi: https://doi.org/10.3390/f14020299.

[18] N. Nuthammachot and D. Stratoulias, "A GIS- and AHP-based approach to map fire risk: a case study of Kuan Kreng peat swamp forest, Thailand," *Geocarto Int.*, vol. 36, no. 2, pp. 212–225, 2021, doi: 10.1080/10106049.2019.1611946;PAGE:STRING:ARTICLE/CHAPTER.

[19] G. S. Ke Jiang, Ran Xing, Zhihan Luo, Wenxuan Huang, Fan Yi, Yatai Men, Nan Zhao, Zhaofeng Chang, Jinfeng Zhao, Bo Pan, "Pollutant emissions from biomass burning: A review on emission characteristics, environmental impacts, and research perspectives," *Particuology*, vol. 85, pp. 296–309, 2024, doi: https://doi.org/10.1016/j.partic.2023.07.012.

[20] L. L. Yifan Cui, "Land-Use Carbon Emissions Estimation for the Yangtze River Delta Urban Agglomeration Using 1994–2016 Landsat Image Data," *Remote Sens*, vol. 10, no. 9, 2018, doi: https://doi.org/10.3390/rs10091334.

[21] M. K. F. B. Abdul Nishar, "Temperature Effects on Biomass and Regeneration of Vegetation in a Geothermal Area," *Front. Plant Sci*, vol. 8, 2017, doi: https://doi.org/10.3389/fpls.2017.00249.

[22] M. Keywood *et al.*, "Fire in the Air: Biomass Burning Impacts in a Changing Climate," *Crit. Rev. Environ. Sci. Technol.*, vol. 43, no. 1, pp. 40–83, 2013, doi: 10.1080/10643389.2011.604248.

[23] S. D. J. Chermelle B. Engel, "Fire Radiative Power (FRP) Values for Biogeographical Region and Individual Geostationary HHMMSS Threshold (BRIGHT) Hotspots Derived from the Advanced Himawari Imager (AHI)," *Remote Sens*, vol. 14, no. 11, 2022, doi: https://doi.org/10.3390/rs14112540.

[24] X. Zhang, S. Kondragunta, and B. Quayle, "Estimation of biomass burned areas using multiple-satellite-observed active fires," *IEEE Trans. Geosci. Remote Sens.*, vol. 49, no. 11 PART 2, pp. 4469–4482, Nov. 2011, doi: 10.1109/TGRS.2011.2149535.

[25] J. R. & Y. Z. Weiyi Xu, Xiaobin Jin, Jing Liu, Xuhong Yang, "Analysis of spatio-temporal changes in forest biomass in China," *J. For. Res.*, vol. 33, pp. 261–278, 2022, doi: https://doi.org/10.1007/s11676-021-01299-8.

[26] X. Y. Yunxiang Jin, "Remote Sensing-Based Biomass Estimation and Its Spatio-Temporal Variations in Temperate Grassland, Northern China," *Remote Sens*, vol. 6, no. 2, 2014, doi: https://doi.org/10.3390/rs6021496.

[27] J. T. Tomi Karppinen, Anu-Maija Sundström, Hannakaisa Lindqvist, Juha Hatakka, "Satellite-based assessment of national carbon monoxide concentrations for air quality reporting in Finland," *Remote Sens. Appl. Soc. Environ.*, vol. 33, p. 101120, 2024, doi: https://doi.org/10.1016/j.rsase.2023.101120.

[28] C. L. Michal Pardo, "Health impacts of biomass burning aerosols: Relation to oxidative stress and inflammation," *Aerosol Sci. Technol.*, vol. 58, no. 10, 2024, [Online]. Available: https://www.tandfonline.com/doi/full/10.1080/02786826.2024.2379551

[29] J. C. Zhan Chen, "Effects of Elevated Ozone Levels on Photosynthesis, Biomass and Non-structural Carbohydrates of Phoebe bournei and Phoebe zhennan in Subtropical China," *Front. Plant Sci.*, 2018, [Online]. Available: https://www.frontiersin.org/journals/plant-science/articles/10.3389/fpls.2018.01764/full